



Impact of High-Strength Reinforcement on Ductility of Normal-Strength Reinforced Concrete Column

#	Name	Email Address	Degree	Country	Affiliation
1	Ulfa, Anis Aulia	anis.aulia@poltekba.ac.id	MD	Indonesia	Civil Engineering, Politeknik Negeri Balikpapan, Balikpapan, Indonesia
2	Piscesa, Bambang	piscesa@ce.its.ac.id	Ph.D.	Indonesia	Civil Engineering Department, Institut Teknologi Sepuluh Nopember

Received: 22/09/2023
Revised: 02/05/2024
Accepted: 29/05/2024

Abstract

The ductility of reinforced concrete columns can be significantly influenced by the configurations and material properties of the confining bars. Extensive research is required to comprehend the limitations on yield strength imposed by certain building codes, particularly concerning high-strength reinforcement. AS3600:2017 and ACI318-19 codes restrict the yield strength of confinement reinforcement to 800 MPa and 700 MPa, respectively. This study investigates the ductility of reinforced concrete columns using five different confining bar configurations, two concrete compressive strengths (30 MPa and 50 MPa), two longitudinal reinforcement yield strengths (420 MPa and 500 MPa), and four transverse reinforcement yield strengths (420 MPa, 500 MPa, 700 MPa, and 1000 MPa). The diameter of the confining bars is adjusted to meet the

required area estimates from ACI318-19 and AS3600:2017 codes. Additionally, finite element analysis is conducted using the 3D-NLFEA package. The results demonstrate the safety and adequate ductility provided by high-strength steel in reinforced concrete columns. Furthermore, a simple formulation for column ductility, which integrates the confining bar configurations, is proposed based on the numerical study.

Keyword: Confinement, configuration, ductility index, 3D-NLFEA, finite element method.

1. Introduction

Sreevalli (2021) have emphasized the need to understand the behavior of reinforced concrete structures under various conditions to ensure safety. For example, the review highlights the importance of analyzing and simulating structural elements to comprehend failure mechanisms and improve design practices (Sreevalli 2021).

Column failure is a critical issue that occurs when a column lacks the ability to resist shear forces and exhibits low ductility, typically due to insufficient confinement requirements. To mitigate the risk of column collapse, it is essential to adopt effective solutions that can delay the failure process in a ductile manner. One such solution is to use lateral reinforcement as concrete column confinement. This technique has been widely recognized as an effective measure to enhance the ductility of concrete columns, delay the onset of failure, and improve the overall structural performance. The collapse of concrete is typically caused by continuous axial loading, leading to uncontrolled volume expansion. However, the expected collapse can be significantly slowed down and controlled by using sufficient confinement to the concrete core. Thus, it is possible to delay the onset of failure and improve the overall structural behavior of the column.

Previous research has delved into the augmentation of stress-strain characteristics in concrete through the use of transverse reinforcement, such as hoops or ties. The findings from Hong Yang Ding's research suggest that the restraining impact of stirrups boosts the peak stress, leading to an improvement in the load-bearing capacity of the specimen. Moreover, the seismic performance of a short column can be elevated by increasing the volume-stirrup ratio and shear span ratio (Ding et al. 2017). These investigations underscore the potential of transverse reinforcement in augmenting axial stress capacity and deformability in reinforced concrete (RC) columns. The overarching aim is to elevate ductility by intensifying stress and strain within the column, consequently delaying the risk of column collapse.

Min-Jun Kim's work showcased a more pronounced ductile response post-flexural yielding with increased yield strength of transverse reinforcement, indicating heightened lateral confinement (Kim et al. 2021) Furthermore, the utilization of high-strength reinforcing bars offers cost-saving benefits while maintaining column strength and ductility (Alavi-Dehkordi and Mostofinejad 2018). When subjected to substantial lateral displacement, the NSS specimen experiences a more pronounced decrease in strength compared to the HSS specimen. Enhancing the strength of the stirrups has minimal impact on the reduction in stiffness (Wang et al. 2020). High-strength reinforcement enables larger pitch spacing of transverse reinforcement, enhancing the workability of concrete during casting.

It's imperative to recognize the limitations imposed by building codes. AS3600:2017 restricts the yield stress of transverse reinforcement to 800 MPa, while ACI 318-19 imposes a limit of 700 MPa (AS:3600 2017) (ACI 318 2019) ACI 318-2019 mandates a minimum level of confinement reinforcement to ensure ductility, whereas AS3600:2017 allows for various design approaches, specifying a minimum effective confining pressure of 0.01 times the concrete strength.

The configuration of transverse reinforcement, including the detailing of hooks, significantly contributes to enhancing concrete core confinement. This aspect plays a crucial role in preventing longitudinal bar buckling. It is essential to explore different transverse reinforcement configurations to understand their impact on confining pressure and, consequently, on both column strain ductility and ductility index.

This study explores the ductility of RC columns crafted from normal-strength concrete and high-strength reinforcement. Beyond this primary objective, the research scrutinizes the influence of various reinforcement configurations and confinement parameters on the ductility of reinforced concrete columns. Moreover, it aims to provide valuable insights into the structural behavior guided by diverse design standards.

2. Material and Methods

This study was the extended research carried out by the author in (Ulfa et al. 2020), by incorporating various confinement configurations. Analysis of the model will be implemented using the finite element method with an in-house 3D-NLFEA package developed by Piscesa et al (Piscesa, Attard, and Samani 2018). The 3D-NLFEA utilizes the plasticity-fracture model for concrete, which is restraint sensitive and incorporates premature cover spalling due to restrained shrinkage (Piscesa et al. 2019). The reinforced concrete (RC) columns designed with high-strength rebar based on ACI 318-19 and AS 3600-2017 will be evaluated for their ductility and axial load carrying capacity. The analysis result of these columns will enable the determination of the peak load and provide insights into the impact of confinement parameters and reinforcement configurations on the ductility index (I_{10}).

High-strength reinforcing bars serve as earthquake-resistant alternatives, offering comparable normalized energy dissipation to standard-strength bars (Kamaruddin, Imran, and Imansyah 2018). However, incorporating high-strength reinforcement reduces the member's stiffness, resulting in increased elastic deformation prior to yielding. On the other hand, Prasetya's test results (Ou and Kurniawan 2015) indicate that transverse reinforcement yielded after the column reached its peak strength. For shear reinforcement Ou et al. Ou recommend a limit of 600 MPa. The AS3600:2017 regulation restricts stirrup reinforcement yield stress to 800 MPa, while ACI 318-19 limits it to 700 MPa.

This study aims to ensure an equal confinement pressure across various reinforcement configurations. Each increase in reinforcement strength corresponds to a distinct confinement pressure, with higher strength leading to greater restraint stress. To maintain uniform confinement pressure, the diameter of the confinement rebar reinforcement is adjusted. The variation in diameter is determined based on the minimum required stirrup reinforcement specified in

AS3600:2017 and ACI 318-2019 regulations. By adhering to these guidelines, the study ensures compliance with design standards while enabling a comprehensive analysis of the impact of confinement pressure on reinforced elements' behavior.

The longitudinal reinforcement area of columns, as per ACI 318-2019, is determined by $A_{st} \geq 0.01 A_g$, where A_g is the column cross-sectional area and A_{st} is the required area of longitudinal reinforcement:

$$A_g = 600 \text{ mm} \times 600 \text{ mm} = 360000 \text{ mm}^2$$

$$A_{st} \geq 0.01 \times 360000 \text{ mm}^2$$

$$\geq 3600 \text{ mm}^2$$

Based on different types of confinement reinforcement configurations, the number of longitudinal bars in Type I and II columns differs from the number in Type III, IV, and V columns. For Type I and II columns with the number of longitudinal bars, $n_b = 8$ and $d_b = 25\text{mm}$ with $\frac{A_{st}}{A_g} = 0.011$.

While for Type III, IV, and V columns with the number of longitudinal bars, $n_b = 12$ and $d_b = 20\text{mm}$ with $\frac{A_{st}}{A_g} = 0.0105$.

As per the guidelines specified in ACI 318-2019 Clause 18.7.5.4, for Normal Strength Concrete with a compressive strength $f'_c \leq 10000 \text{ psi}$ (i.e. 68.94757 Mpa) the requirement for transverse reinforcement dictates that $A_{sh}/(b.s)$ should meet or exceed the criteria outlined in equations (1) and (2) as follows:

$$\frac{A_{sh}}{b_c s} = 0,3 \left(\frac{A_g}{A_{ch}} - 1 \right) \frac{f'_c}{f_{yt}} \quad (1)$$

$$\frac{A_{sh}}{b_c s} = 0,09 \frac{f'_c}{f_{yt}} \quad (2)$$

$$A_{sh} = n_s \frac{1}{4} \pi d^2 \quad (3)$$

Where A_g is the gross area of the column cross-section, A_{ch} is the centre-to-centre bounded core area of the longitudinal reinforcement, b is the overall width of the column, and s is the distance between the confining bars along the column.

According to AS3600 (2017), the triaxial stress across all sections and the effectiveness of confining bars are used to obtain the confining pressure in the core (Samani, Attard, and Foster 2015). Clause 10.7.3.3, the effective stress confinement ($f_{r,eff}$) is:

$$f_{r,eff} = k_e, f_r \geq 0.01 f'_c \quad (4)$$

$$k_e = \left(1 - \frac{n, w^2}{6, A_c}\right) \left(1 - \frac{s}{2, b_c}\right) \left(1 - \frac{s}{2, d_c}\right) \quad (5)$$

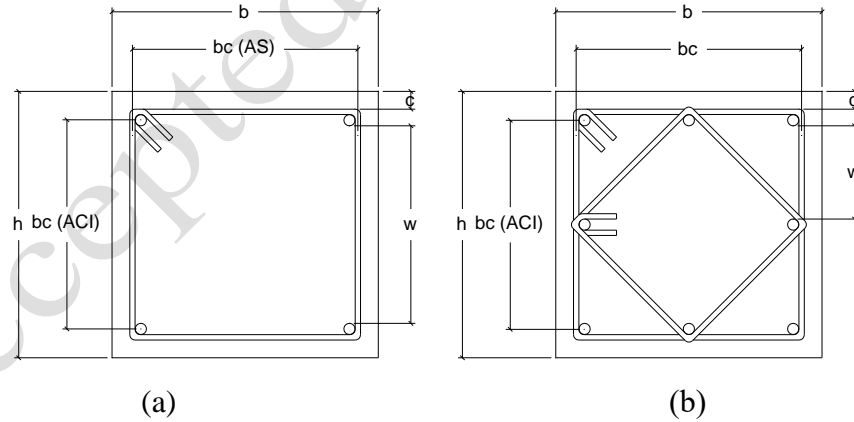
Where k_e is the effectiveness factor of the reinforcement confinement and f_r is the confinement stress that can be calculated using the following equation:

$$f_r = \frac{\sum_{i=1}^m A_{bf_{it}} \cdot f_{syf} \sin \theta}{d_s \cdot s} \quad (6)$$

$$\sum_{i=1}^m A_{bf_{it}} \cdot \sin \theta = \frac{f_r \cdot d_s \cdot s}{f_{syf}} \quad (7)$$

n is the number of longitudinal reinforcements, w is the average net distance among adjacent longitudinal reinforcements, b_c and d_c are the centre-to-centre measurements of outermost reinforcement, and A_c is the core area bounded by the centre-to-centre of the outermost confinement. $A_{bf_{it}}$ is the cross-sectional area of one bar, f_{syf} is the yield stress of the lateral reinforcement, m is the number of legs intersecting the confinement section, θ is the angle between the reinforcing tie to the plane, and d_s is the dimension measured from the centre-to-centre of the outer confinement reinforcement.

Square column confinement is more effective than that of rectangular columns. Hence, this study examines the ductility of square-reinforced concrete columns through analysis of five different configurations. Figure 1 illustrates these configurations. A total of 120 square reinforced concrete columns were used in the study, each measuring 600 mm x 600 mm x 1800 mm. The columns feature a concrete cap that is 40 mm thick and have a pitch spacing of 100 mm.



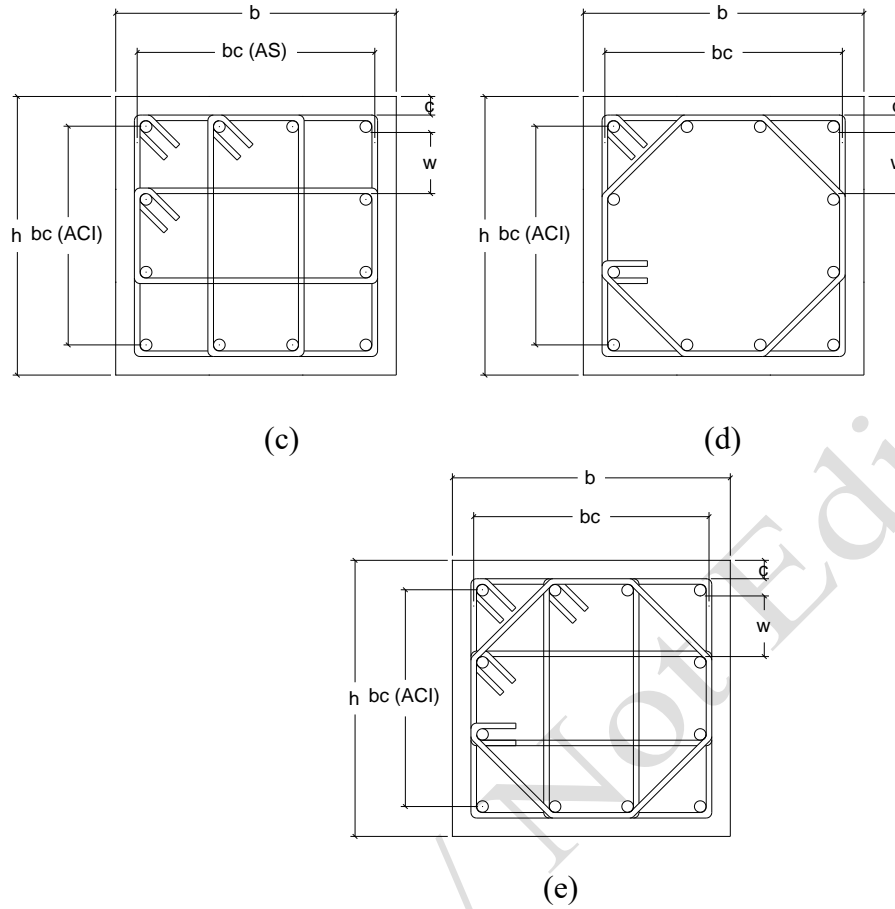


Figure 1. Confinement configuration of the test specimen
 (a) Type 1, (b) Type 2, (c) Type 3, (d) Type 4, (e) Type 5.

The test specimens based on the material's strength are labelled as shown in Tables 1 and 2.

Table 1. Labelling of Column Specimens (f'_c 30 MPa)

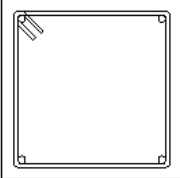
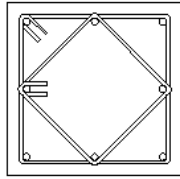
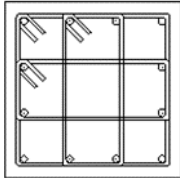
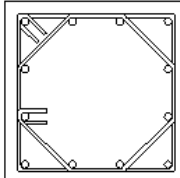
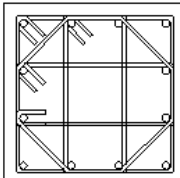
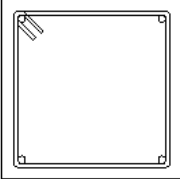
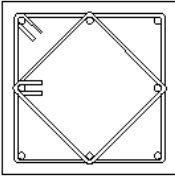
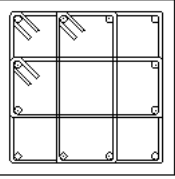
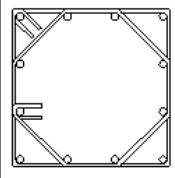
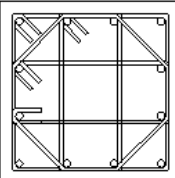
Compressive strength of concrete (f'_c)	30 MPa						
	Longitudinal rebar yield strength (f_y)	420 MPa			500 MPa		
		420 MPa	700 MPa	1000 MPa	500 MPa	700 MPa	1000 MPa
Transversal rebar yield strength (f_{yt})	420 MPa	700 MPa	1000 MPa	500 MPa	700 MPa	1000 MPa	
	I3.L4.T4	I3.L4.T7	I3.L4.T10	I3.L5.T5	I3.L5.T7	I3.L5.T10	
	II3.L4.T4	II3.L4.T7	II3.L4.T10	II3.L5.T5	II3.L5.T7	II3.L5.T10	
	III3.L4.T4	III3.L4.T7	III3.L4.T10	III3.L5.T5	III3.L5.T7	III3.L5.T10	
	IV3.L4.T4	IV3.L4.T7	IV3.L4.T10	IV3.L5.T5	IV3.L5.T7	IV3.L5.T10	
	V3.L4.T4	V3.L4.T7	V3.L4.T10	V3.L5.T5	V3.L5.T7	V3.L5.T10	

Table 2. Labelling of Column Specimens (f'_c 50 MPa)

Compressive strength of concrete (f'_c)	50 MPa					
Longitudinal rebar yield strength (f_y)	420 MPa			500 MPa		
Transversal rebar yield strength (f_{yt})	420 MPa	700 MPa	1000 MPa	500 MPa	700 MPa	1000 MPa
	I5.L4.T4	I5.L4.T7	I5.L4.T10	I5.L5.T5	I5.L5.T7	I5.L5.T10
	II5.L4.T4	II5.L4.T7	II5.L4.T10	II5.L5.T5	II5.L5.T7	II5.L5.T10
	III5.L4.T4	III5.L4.T7	III5.L4.T10	III5.L5.T5	III5.L5.T7	III5.L5.T10
	IV5.L4.T4	IV5.L4.T7	IV5.L4.T10	IV5.L5.T5	IV5.L5.T7	IV5.L5.T10
	V5.L4.T4	V5.L4.T7	V5.L4.T10	V5.L5.T5	V5.L5.T7	V5.L5.T10

The label can be interpreted as follows: Specimen I3.L4.T4. The Roman numeral I represents the specimen configuration type, number 3 indicates the compressive strength of concrete (Type 3 for 30 MPa and Type 5 for 50 MPa), L4 signifies the strength of longitudinal reinforcement at 420 MPa, and T4 denotes the type of transverse reinforcement at 420 MPa.

Concrete under effective confinement exhibits full arching action, primarily expressed within the core area of the concrete. Additionally, each confinement configuration generates a distinct confinement pressure, influenced by the quantity and arrangement of the confining bars. The

calculation of confinement pressure involves analyzing the cross-section's free body, enabling the determination of f_r and $A_{b,fit}$ based on the equilibrium stress illustrated in Figure 2.

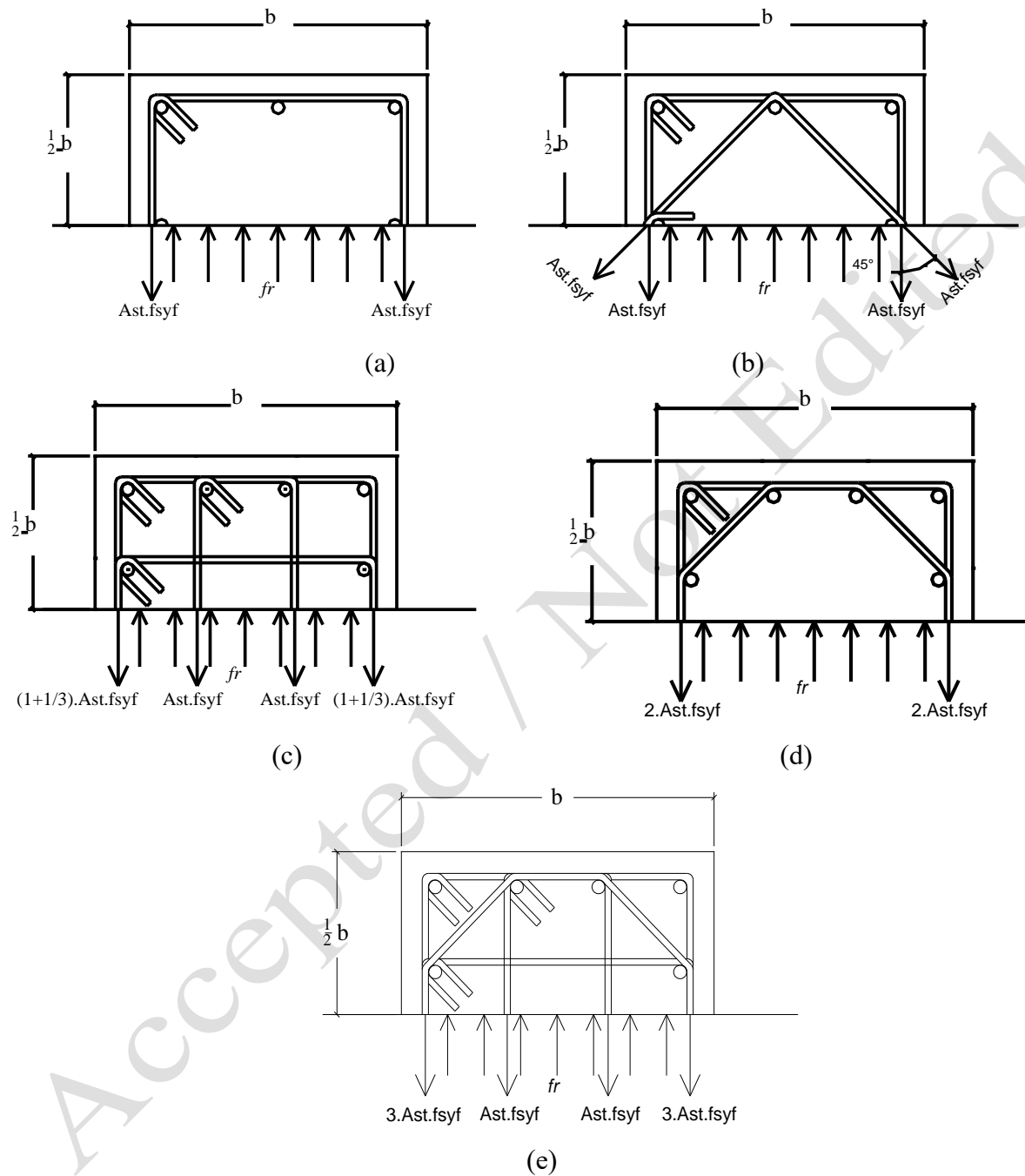


Figure 2. The effect of confinement configuration on the concrete confinement pressure in the test specimens (a) Type 1, (b) Type 2, (c) Type 3, (d) Type 4, (e) Type 5.

Table 3 presents the influence of the confining bar on the concrete confinement pressure and the number of tie legs in each confinement configuration, as depicted in Figure 2.

Table 3 The Number of Tie Legs Each Configuration

Column Type	I	II	III	IV	V
Tie Legs	2	3.414	4.667	3.61	6.28

The specimens consist of normal strength concrete with compressive strengths of 30 MPa and 50 MPa, along with high strength steel confining bars. These specimens are varied based on the strengths of longitudinal and transverse reinforcements. The variations are as follows: (a) Longitudinal reinforcement yield strength (f_y) of 420 MPa, with confinement yield strengths (f_{yt}) of 420 MPa, 700 MPa, and 1000 MPa. (b) Longitudinal reinforcement yield strength (f_y) of 500 MPa, with confinement yield strengths (f_{yt}) of 500 MPa, 700 MPa, and 1000 MPa.

The stress-strain behavior of the longitudinal reinforcement is assumed to be perfectly elastic-plastic. For the lateral reinforcement, stress-strain models from various research journals are employed: (1) Seliem (Seliem et al. 2009) is referenced for confining steel rebar with a yield strength $f_{yt} = 420$ MPa; (2) Nehrp (Moehle et al. n.d.) provides the stress-strain model for confining steel rebar with a yield strength $f_{yt} = 500$ MPa; (3) Hung (Hung and Chueh 2016) is consulted for the stress-strain model of confining steel rebar with a yield strength $f_{yt} = 700$ MPa and (4) Cai (Cai, Wang, and Yang 2018) is utilized for the stress-strain model of confining steel rebar with a yield strength $f_{yt} = 1000$ MPa. Figure 3 depicts the stress-strain diagram of the confining steel rebar.

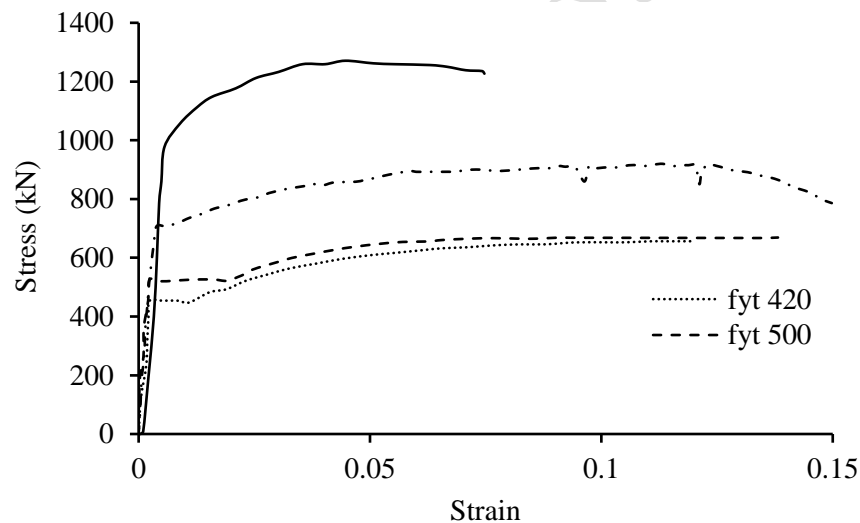


Figure 3 Stress-strain Diagram of Lateral Reinforcement.

To comply with the requirements of ACI 318-2019 Clause 18.7.4.1, which mandates $A_{st} \geq 0.01 A_g$ for the longitudinal reinforcement area, the following design decisions were made:

- Type I and II columns have a reinforcement diameter of 25 mm, equivalent to 1.09% of the gross cross-sectional area.
- Type III, IV, and V columns feature a 20 mm longitudinal reinforcement diameter, representing 1.05% of the gross cross-sectional area.

These design choices ensure adherence to the specified longitudinal reinforcement area requirements.

Each specimen will be analyzed by systematically adjusting the diameter of the confining rebar, taking into account the minimum diameter criteria specified in AS3600-2017 and ACI 318-2019.

The material properties of the columns include a presumed density of 2200 kg/cm³ and a Young's modulus of 200,000 MPa for the reinforcement.

Furthermore, by using equation (3), the diameter of the transverse reinforcement is analytically determined to meet the required area specifications stated in equations (1) and (2). The values of k_e and f_r vary based on the number of longitudinal reinforcements and their corresponding A_s values, leading to specific calculations. For column samples designed according to AS3600 standards (with a minimum $f_r:eff = 0.01 f_c$), the values of k_e and f_r can be computed using equations (4) and (5) respectively, and the results are summarized in Table 4.

Table 4 k_e and f_r Correspond to The Number of Longitudinal Bar

Column Type	I & II	III, IV & V
k_e	0.62214	0.68935
f_r (30 MPa)	0.48221	0.43519
f_r (50 MPa)	0.80368	0.72532

ACI 318-2019 provides guidelines for the area of confinement reinforcement based on equation (3), while AS 3600-2017 enables the calculation of the required diameter of the confinement rebar using equation (7) to satisfy the minimum $f_r:eff$ requirements. Table 5 presents the obtained reinforcement diameters for each specimen based on the requirements specified in AS 3600-2017 and ACI 318-2019. It is important to note that the structural frame design in AS 3600-2017 is specifically intended for ordinary to intermediate resisting moment frames (OMRF to IMRF), while the ACI 318-19 confinement equation is intended for special resisting moment frames (SRMF).

Table 5 Minimum confinement rebar diameter (mm) of specimen

Column Type	AS 3600-2017					ACI 318-19				
	I	II	III	IV	V	I	II	III	IV	V
X3.L4.T4	6.13	4.69	3.81	4.33	3.29	14.59	11.17	9.60	10.92	8.28
X3.L4.T7	4.75	3.63	2.95	3.36	2.55	11.30	8.651	7.44	8.46	6.41
X3.L4.T10	3.97	3.04	2.47	2.81	2.13	9.46	7.238	6.22	7.08	5.37
X3.L5.T5	5.62	4.3	3.49	3.97	3.01	13.37	10.24	8.80	10.01	7.59
X3.L5.T7	4.75	3.63	2.95	3.36	2.55	11.30	8.651	7.44	8.46	6.41
X3.L5.T10	3.97	3.04	2.47	2.81	2.13	9.46	7.238	6.22	7.08	5.37
X5.L4.T4	7.91	6.06	4.92	5.6	4.24	18.84	14.42	12.4	14.1	10.7
X5.L4.T7	6.13	4.69	3.81	4.33	3.29	14.59	11.17	9.60	10.92	8.28
X5.L4.T10	5.13	3.92	3.19	3.63	2.75	12.21	9.344	8.03	9.14	6.93
X5.L5.T5	7.25	5.55	4.51	5.13	3.89	17.26	13.21	11.36	12.92	9.8
X5.L5.T7	6.13	4.69	3.81	4.33	3.29	14.59	11.17	9.603	10.92	8.28
X5.L5.T10	5.13	3.92	3.19	3.63	2.75	12.21	9.344	8.034	9.14	6.93

X indicating the specific configuration type according to the corresponding column type outlined in Table 1 and Table 2.

Figure 4 displays a 3D mesh model of column specimens, which comprises solid elements representing concrete, along with five different reinforcement configurations. The mesh model was created using SALOME 9.2.0 software. The column core and cover regions are clearly differentiated, as illustrated in Figure 4 (a). In the analysis, the load is applied to the top surface of the column, while the bottom surface is fixed as a restraint.

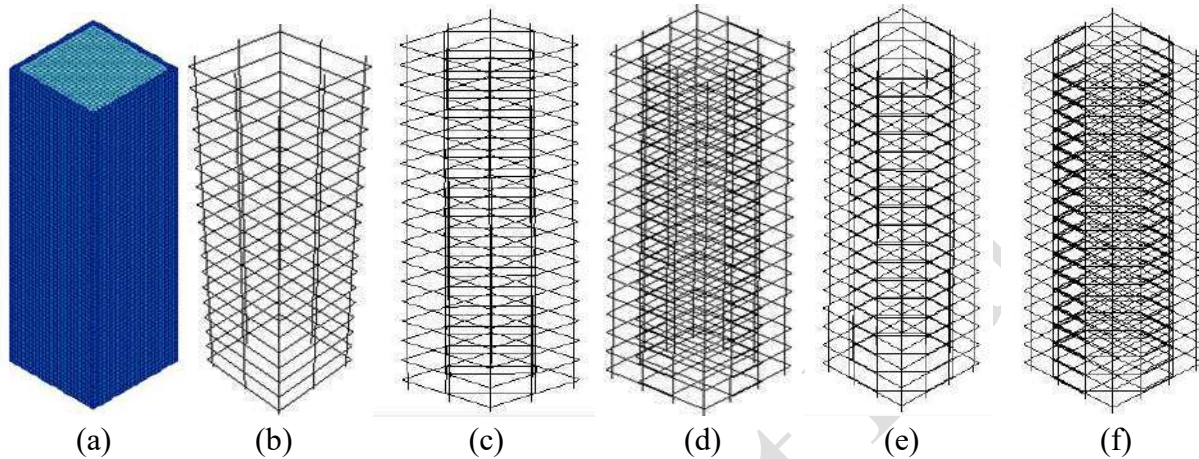


Figure 4 Modeling of Specimens (a) Concrete, (b) Type I, (c) Type II, (d) Type III, (e) Type IV, (f) Type V

3. Results and Discussion

The 3D-NLFEA simulation provides data on load and deformation. These values are then used to calculate the axial stress by dividing the load by the cross-sectional area of the column. Similarly, the axial strain is determined by dividing the deformation by the original length of the column. The resulting stress-strain diagram of the column is depicted in Figure 5–14.

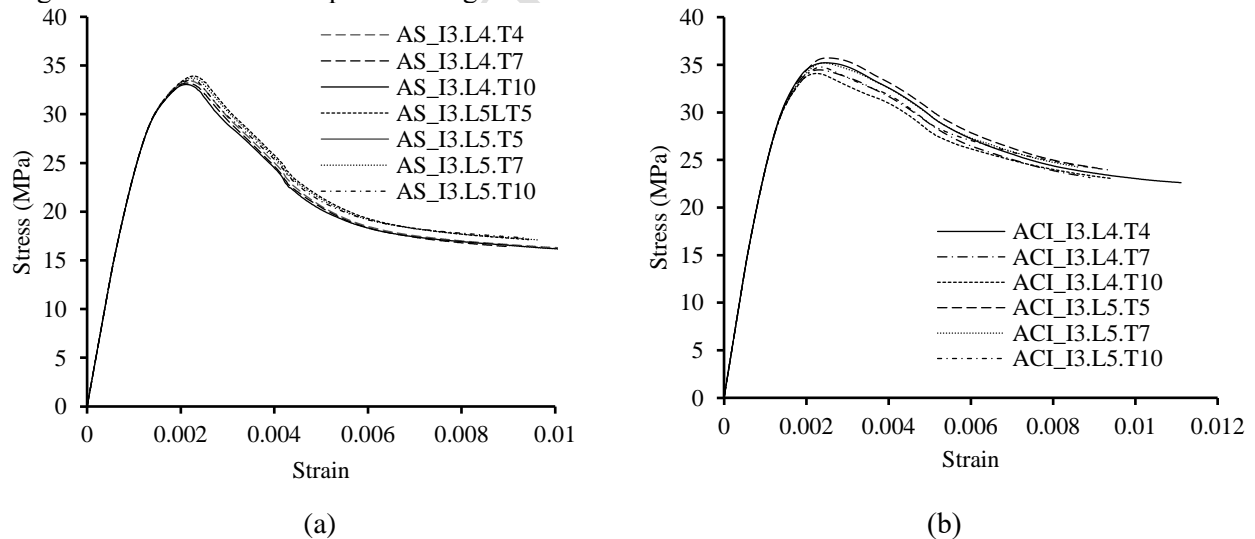
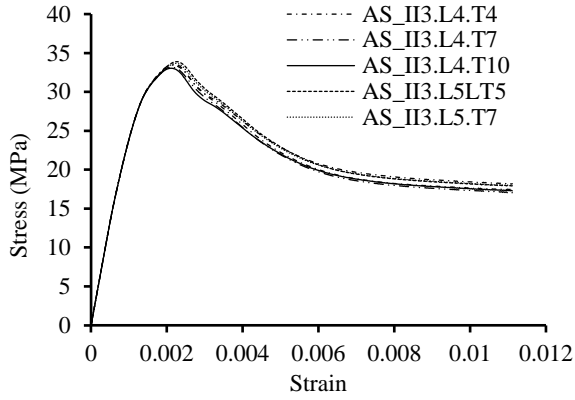
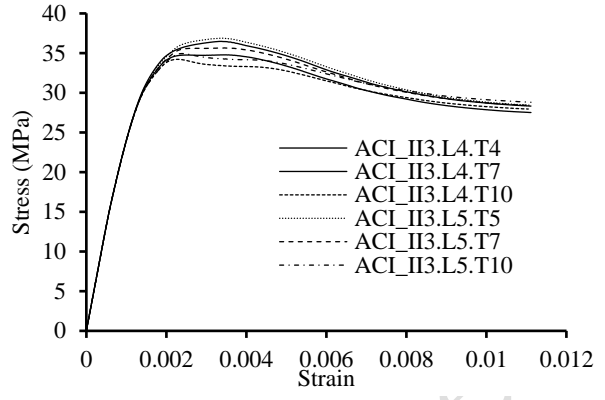


Figure 5 Specimen stress-strain Diagram Type I f'_c 30 MPa (a) AS 3600-2017 (b) ACI 318-2019

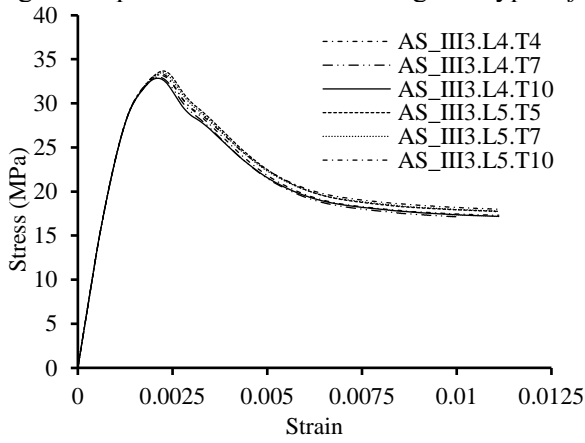


(a)

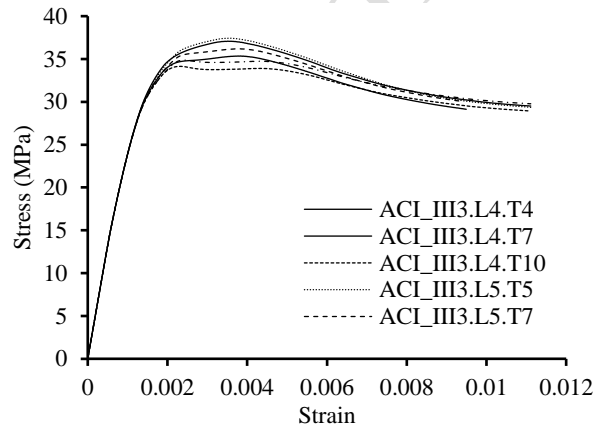


(b)

Figure 6 Specimen stress-strain Diagram Type II f'_c 30 MPa (a) AS 3600-2017 (b) ACI 318-2019

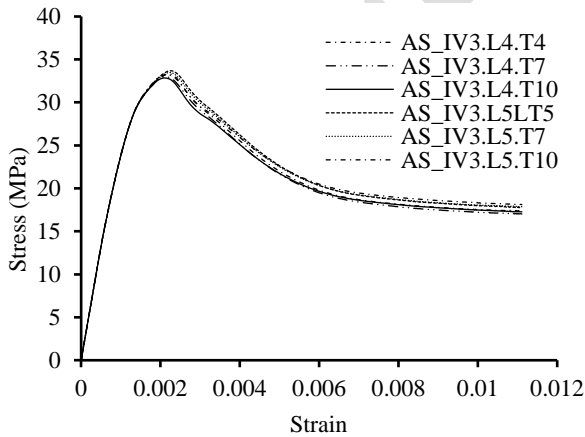


(a)

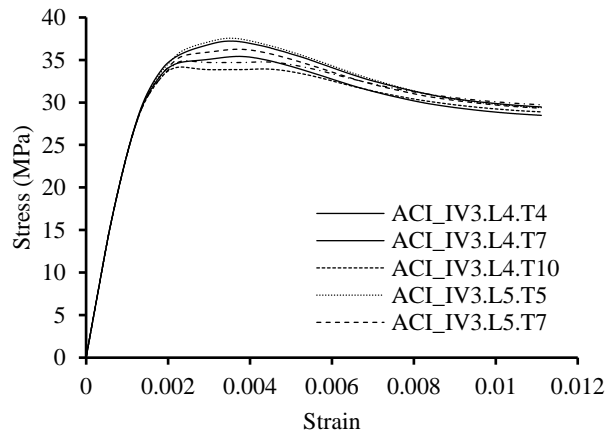


(b)

Figure 7 Specimen stress-strain Diagram Type III f'_c 30 MPa (a) AS 3600-2017 (b) ACI 318-2019

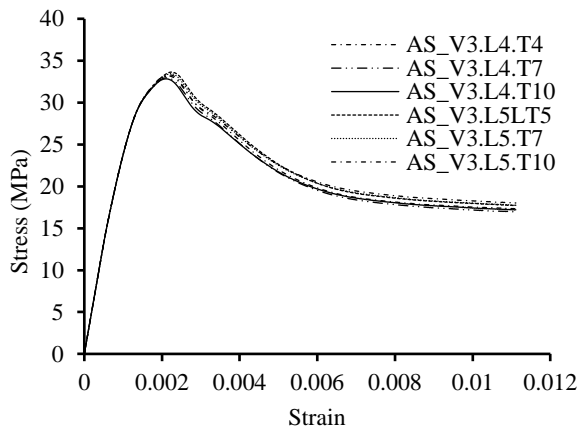


(a)

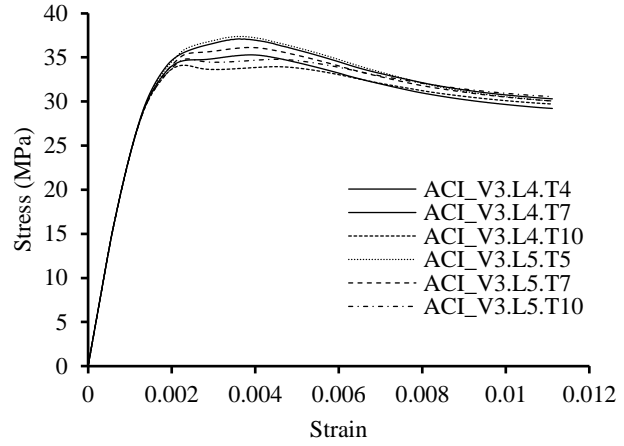


(b)

Figure 8 Specimen stress-strain Diagram Type IV f'_c 30 MPa (a) AS 3600-2017 (b) ACI 318-2019

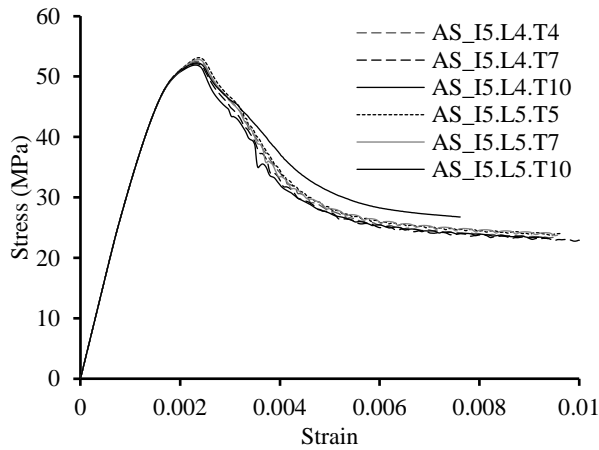


(a)

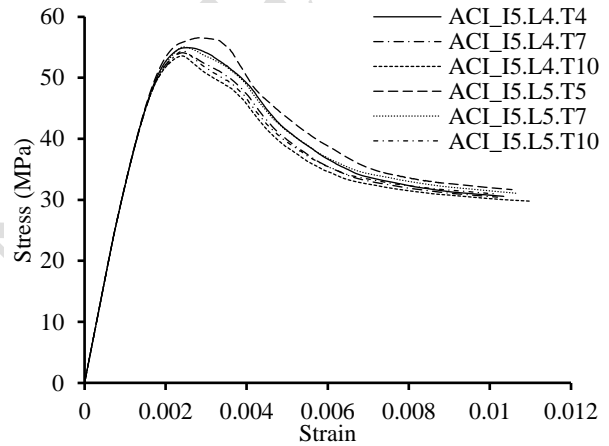


(b)

Figure 9 Specimen stress-strain Diagram Type V f'_c 30 MPa (a) AS 3600-2017 (b) ACI 318-2019

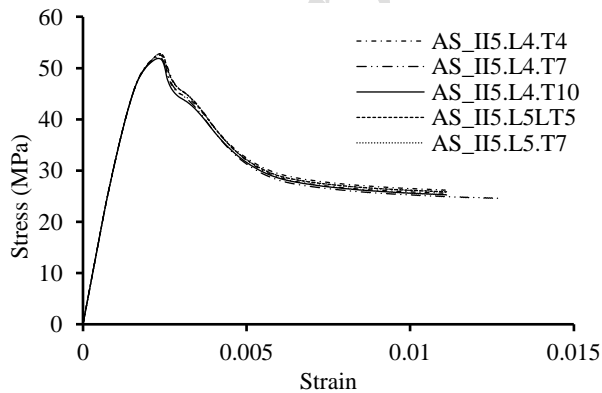


(a)

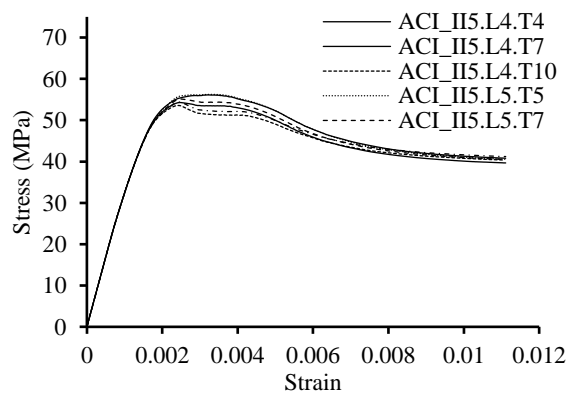


(b)

Figure 10 Specimen stress-strain Diagram Type I f'_c 50 MPa (a) AS 3600-2017 (b) ACI 318-2019

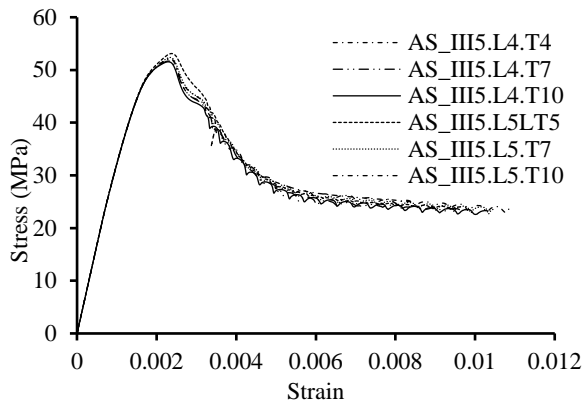


(a)

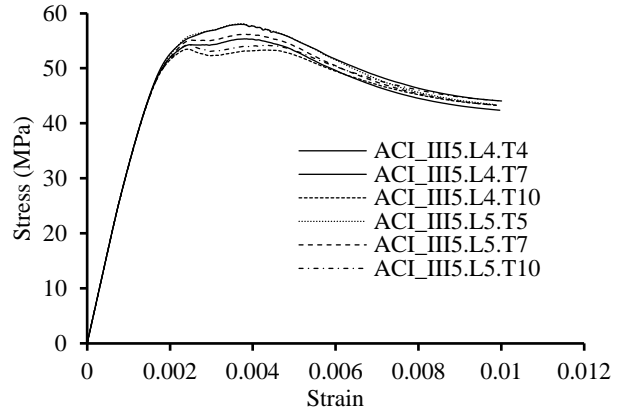


(b)

Figure 11 Specimen stress-strain Diagram Type II f'_c 50 MPa (a) AS 3600-2017 (b) ACI 318-2019

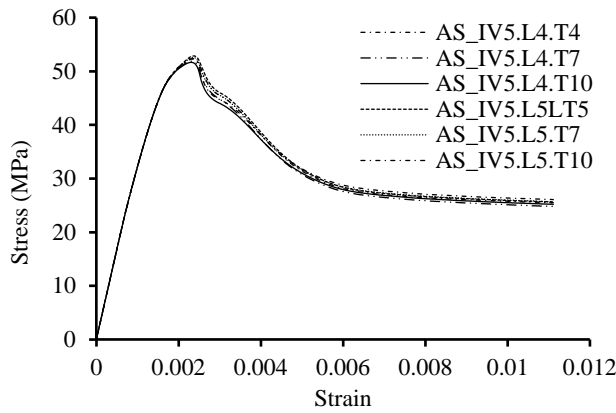


(a)

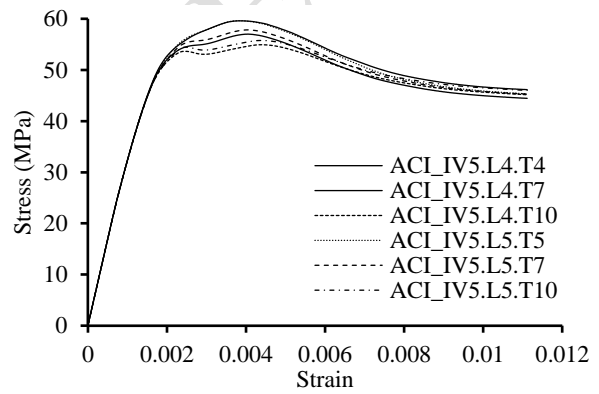


(b)

Figure 12 Specimen stress-strain Diagram Type III f'_c 50 MPa (a) AS 3600-2017 (b) ACI 318-2019

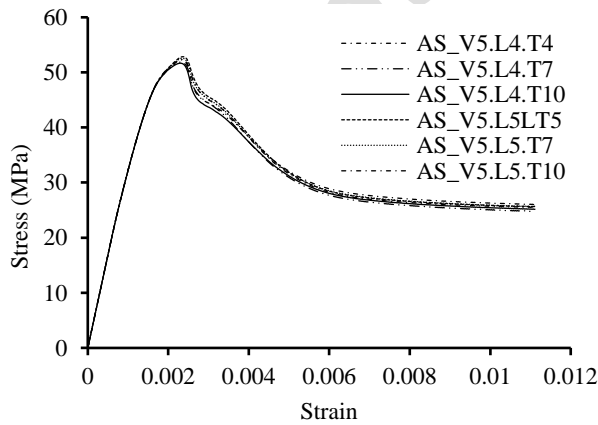


(a)

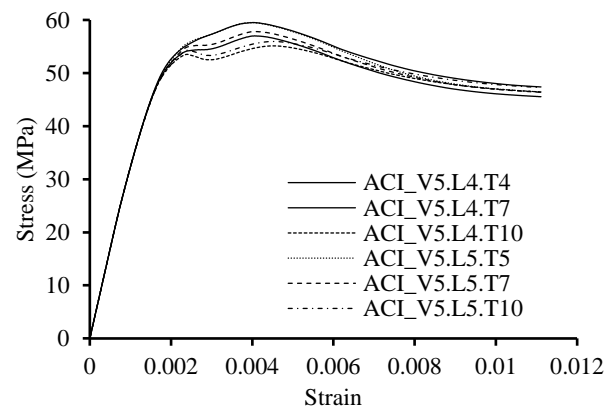


(b)

Figure 13 Specimen stress-strain Diagram Type IV f'_c 50 MPa (a) AS 3600-2017 (b) ACI 318-2019



(a)



(b)

Figure 14 Specimen stress-strain Diagram Type V f'_c 50 MPa (a) AS 3600-2017 (b) ACI 318-2019

Figures 5 to 14 demonstrate that columns with the minimum reinforcement exhibit a similar strain-stress relationship within the same configuration type. The peak stress values for the test specimens are presented in Tables 6 and 7.

Table 6 Peak stress of RC column with constant A_{sh}/bs ratio (ACI-318 2019)

Column Type	I	II	III	IV	V
X3.L4.T4	35.22	36.46	37.08	37.21	37.10
X3.L4.T7	34.47	34.77	35.35	35.41	35.29
X3.L4.T10	34.09	34.20	34.14	34.16	34.11
X3.L5.T5	35.73	36.87	37.43	37.55	37.39
X3.L5.T7	34.47	35.64	36.19	36.25	36.13
X3.L5.T10	34.77	34.92	34.87	34.89	34.83
X5.L4.T4	54.93	56.12	58.00	59.59	59.52
X5.L4.T7	54.10	54.28	55.35	56.99	57.01
X5.L4.T10	53.58	53.56	53.47	54.92	55.13
X5.L5.T5	56.57	56.25	58.12	59.63	59.53
X5.L5.T7	55.06	55.12	56.20	57.82	57.83
X5.L5.T10	54.38	54.39	54.27	55.75	55.96

Table 7 Peak stress of RC column with constant *confining pressure* (AS 3600:2017)

Column Type	I	II	III	IV	V
X3.L4.T4	33.46	33.45	33.23	33.24	33.21
X3.L4.T7	33.20	33.18	32.97	32.98	32.96
X3.L4.T10	33.06	33.04	32.84	32.84	32.83
X3.L5.T5	33.91	33.88	33.67	33.68	33.65
X3.L5.T7	33.72	33.67	33.48	33.48	33.46
X3.L5.T10	33.53	33.51	33.31	33.32	33.31
X5.L4.T4	52.53	52.53	52.02	52.32	52.27
X5.L4.T7	52.11	52.10	51.69	51.89	51.86
X5.L4.T10	52.27	51.89	51.55	51.68	51.65
X5.L5.T5	53.12	53.11	53.12	52.88	52.83
X5.L5.T7	52.84	52.81	52.37	52.59	52.55
X5.L5.T10	51.89	52.57	52.21	52.36	52.32

Figures 15 demonstrates the influence of varying the yield stress of longitudinal reinforcement (f_y) and confinement reinforcement (f_{yt}) on the peak stress of column type 1.

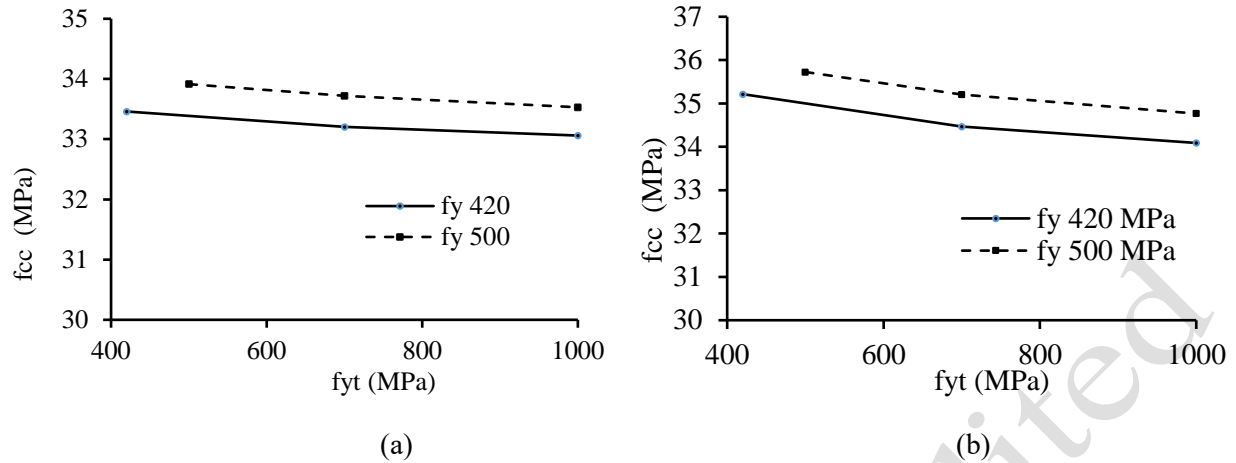


Figure 15 Peak Stress of Column Type I with f_y dan f_{yt} Variation (a) AS 3600-2017 (b) ACI 318-2019

Figure 15 illustrates that a column featuring 500 MPa longitudinal reinforcement exhibits a higher peak stress compared to a column with 420 MPa longitudinal reinforcement. This distinction arises from the initial planning phase, where the diameter of the longitudinal reinforcement is kept constant within each configuration type. However, columns that employ longitudinal reinforcement with higher yield stresses will exhibit greater strength due to the amplified restraint effects resulting from varying yield stresses of the transverse reinforcement.

The column's peak stress variation is influenced by the lateral stiffness, which depends on the stirrup reinforcement diameter. Stirrups with lower yield stresses have larger bar diameters, resulting in increased lateral stiffness. Equations (8) and (9) can be utilized for calculating the lateral stiffness of a restraint:

$$L_{atstiff} = \frac{E_s A_{b,fit}}{L_{tieleg}} \quad (8)$$

$$L_{tieleg} = n_{tieleg} \frac{1}{2} b_c \quad (9)$$

The lateral stiffness of the column can be observed in Table 8.

Table 8 Lateral Stiffness of Specimen Type I f'_c 30 MPa

	Lateral Stiffness	
	AS	ACI
I3.L4.T4	11481,095	71005,917
I3.L4.T7	6888,657	42603,550
I3.L4.T10	4822,060	29822,485
I3.L5.T5	9644,119	59644,970
I3.L5.T7	6888,657	42603,550
I3.L5.T10	4822,060	29822,485

The disparity in confinement pressure between columns designed according to AS3600:2017 and ACI 318-2019 has a notable impact on the lateral stiffness. Columns designed under ACI 318-2019 exhibit a lateral stiffness approximately six times greater than those designed under AS3600:2017. Consequently, columns designed per AS3600:2017 experience a more rapid decline in stress after reaching the peak compared to columns designed according to ACI 318-2019 standards.

Following the previous explanation, Figure 16 illustrates the comparison of peak stress among columns with a compressive strength of 30 MPa (f'_c), longitudinal reinforcement yield stress (f_y) of 420 MPa and the confinement yield stress (f_{yt}) of 420 MPa for each configuration.

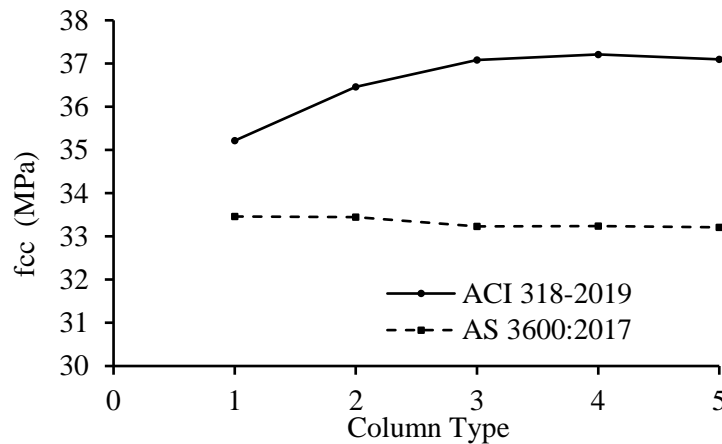


Figure 16 Comparison of f_{cc} Column with f'_c 30 MPa, f_y 420 Mpa and f_{yt} 420 Mpa Each Configuration

In Figure 16, columns type I and II designed according to AS 3600:2017 show similar peak stresses due to their comparable reinforcement ratios. Similarly, columns III, IV, and V exhibit nearly identical peak stresses. Figure 17 illustrates the stress-strain relationship of the AS_I3.L4.T4 column, with a longitudinal reinforcement ratio of 0.0105, obtained from additional simulations for comparison.

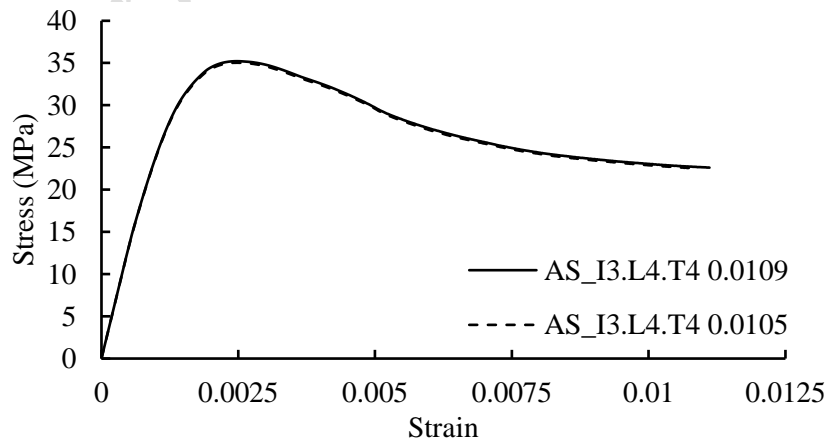


Figure 17. AS_I3.L4.T4 column stress-strain comparison between 0.0109 and 0.0105 longitudinal reinforcement ratio

Figure 17 compares the stress-strain relationship between two columns: AS_I3.L4.T4 with a longitudinal reinforcement ratio of 0.0109 and AS_I3.L4.T4 with a longitudinal reinforcement ratio of 0.0105. The results show that the ductility and ductility index are not significantly different. However, columns type I and II can achieve peak stresses similar to columns III, IV, and V by adjusting the longitudinal reinforcement ratio. Table 10 displays the peak stresses of columns with f_c 30 MPa, f_y 420 MPa, and f_{yt} 420 MPa for each configuration. Additionally, Figure 18 compares the maximum f_c 30 MPa of each configuration with a longitudinal reinforcement ratio of 0.0105.

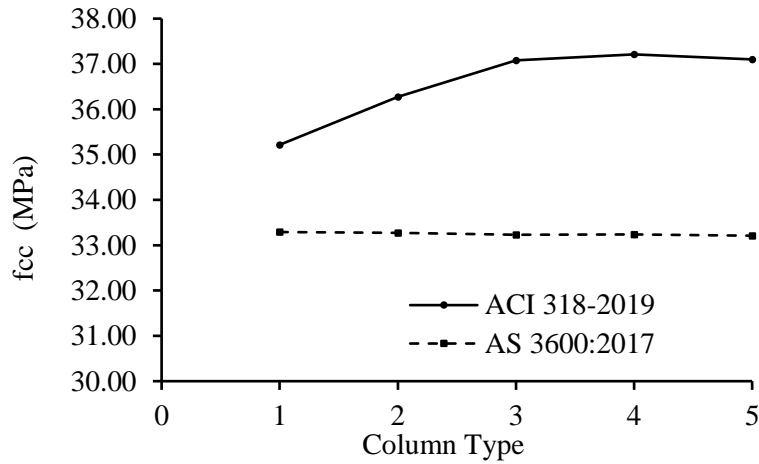


Figure 18 Comparison of f_{cc} Column with f_c 30 MPa, f_y 420 Mpa and f_{yt} 420 Mpa Each Configuration with Longitudinal Reinforcement 0.0105

Columns designed according to ACI 318-2019 exhibit distinct peak stress compared to those designed according to AS 3600:2017. This disparity can be attributed to the differences in the formulations used by AS 3600:2017 and ACI 318-2019 to determine the requirements for confinement reinforcement.

The columns designed according to AS3600:2017 comply $A_{b,fit}$ in equation (10) with the specified confinement requirements, where f_{reff} equal to $0,01 f_c$ as indicated in equations (4) to (7)):

$$A_{b,fit} = \frac{0.01 f_c d_s \cdot s}{k_e f_{sf}} \quad (10)$$

Meanwhile, columns designed according to ACI 318-2019 adhere $A_{b,fit}$ in equation (11) and (12) to the confinement reinforcement requirements specified in equations (1) to (3) below:

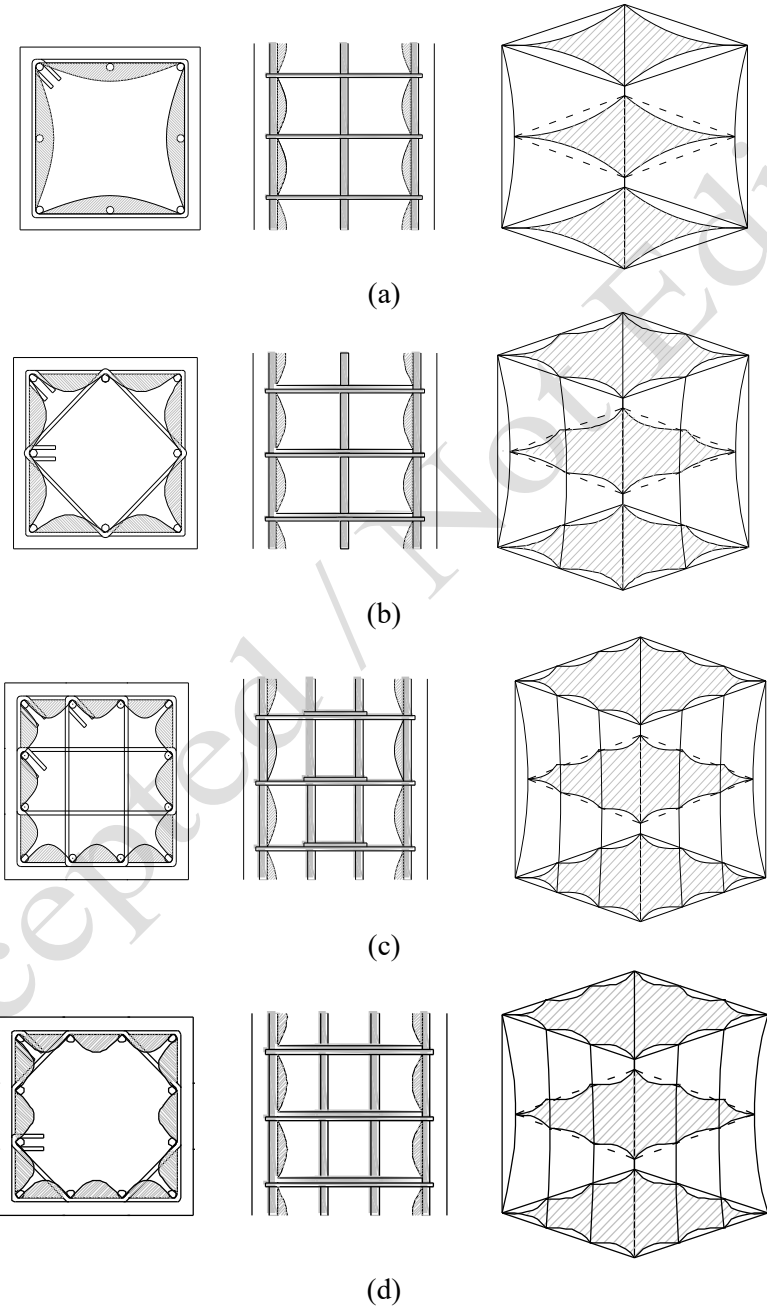
$$A_{b,fit} = \rho \cdot b \cdot s \quad (11)$$

$$A_{b,fit} = \rho \cdot b \cdot s = 0.3 \left(\frac{A_g}{A_{ch}} - 1 \right) \frac{f_c}{f_{sf}} b \cdot s \quad (12)$$

The above equations demonstrate the contrasting approaches of the two codes. AS 3600:2017 incorporates the effective arrangement of longitudinal and transverse reinforcement, considering triaxial confinement. On the other hand, ACI 318-2019 takes into account the ratio between the

gross cross-sectional area and the core column's cross-sectional area when determining the need for confinement reinforcement.

As a result, columns designed according to the transverse reinforcement requirements of AS 3600:2017 exhibit similar peak stresses. In contrast, columns designed following the standards of ACI 318-2019 show negligible variations in peak stress, which are influenced by the core effective volume and configuration type, as depicted in Figure 19.



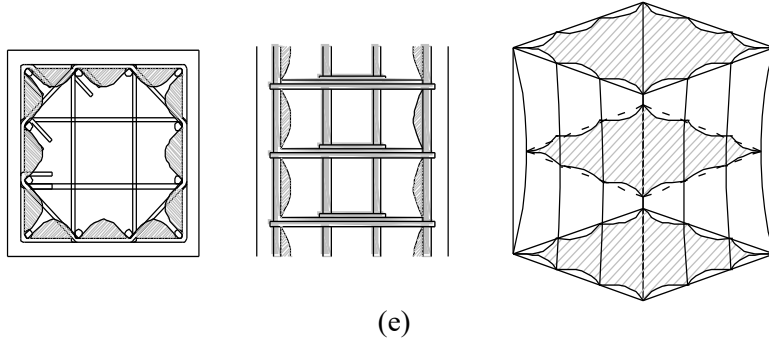


Figure 19 Effect of stirrup configuration on the concrete confinement area (a) Type 1, (b) Type 2, (c) Type 3, (d) Type 4, (e) Type 5.

Figure 20 illustrates a comparison of the peak stress attainment for columns designed to comply with the minimum diameter specifications of ACI 318-2019 and AS 3600:2017.

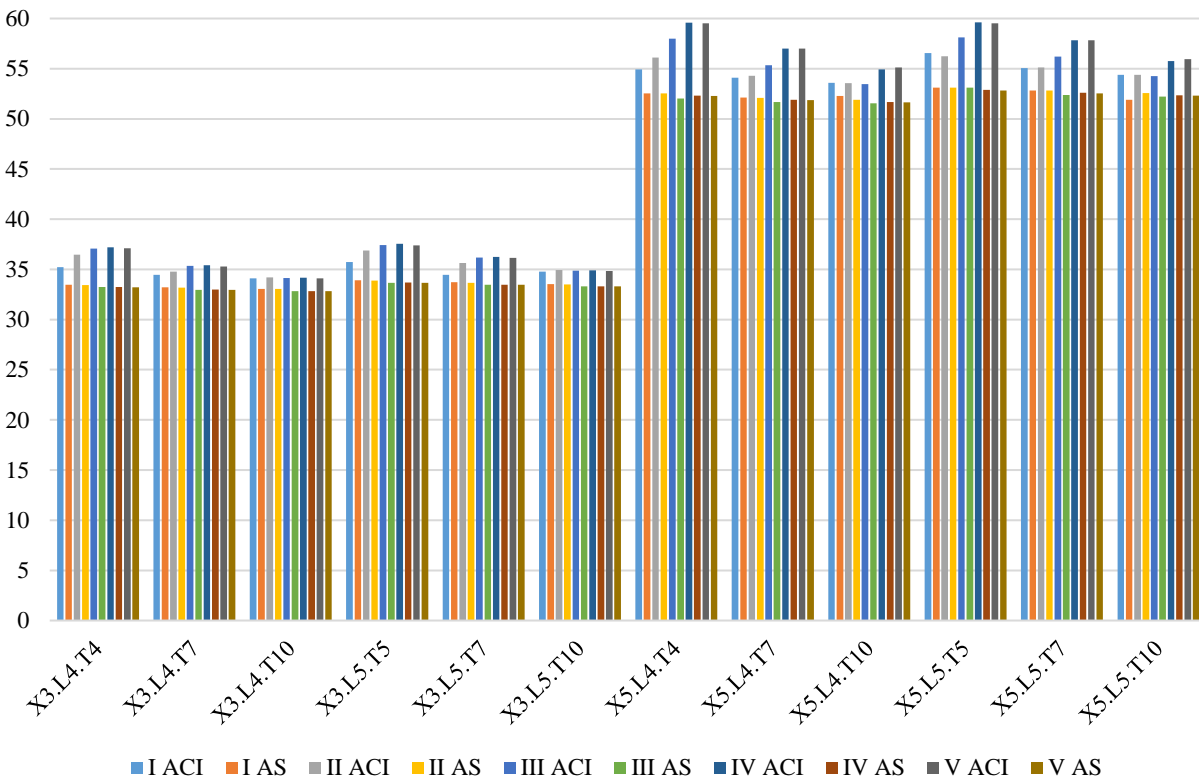


Figure 20 Comparison of the peak stress attainment for columns designed to ACI 318-2019 and AS 3600:2017

Figure 20 reveals insights into the performance of reinforced concrete columns under varying design parameters. Notably, columns featuring 500 MPa longitudinal reinforcement exhibit higher peak stresses compared to their 420 MPa counterparts, emphasizing the substantial influence of longitudinal reinforcement yield strength on overall column strength. The lateral stiffness, determined by stirrup reinforcement diameter, proves to be a critical factor, with lower-yield-stress stirrups exhibiting larger bar diameters and increased lateral stiffness. Moreover, the observed

disparities in confinement pressure between AS3600:2017 and ACI 318-2019-designed columns significantly impact lateral stiffness, leading to distinct stress distribution patterns. The nuanced variations in peak stress, particularly in columns designed per ACI 318-2019, underscore the importance of understanding and optimizing column behavior based on specific code requirements and design objectives.

Ductility is associated with the configuration of a structural system or member and its section behavior. The ductility of the test specimen column I3.L4.T4, designed according to the reinforcing requirements specified in the AS 3600:2017 standard, can be assessed using the graphical approach depicted in Figure 20.

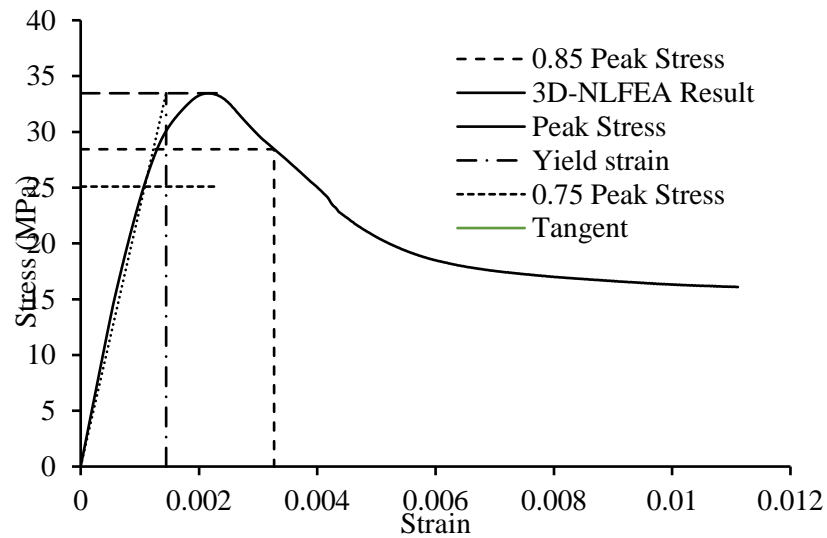


Figure 21 Ductility Calculation of Column Type I3.L4.T4 Designed According to ACI 318-2019

In Figure 21, the yield strain of the column is determined by drawing tangents from coordinates 0.0 and 0.75 to the peak stress value. For column I3.L4.T4, the yield strain is obtained at the intersection of the tangent with the peak stress. Additionally, the concrete reaches its ultimate strain when the stress is reduced to 15% of the peak stress. Therefore, the ductility can be calculated using equation (13) as follows:

$$\mu = \frac{\epsilon_u}{\epsilon_y} \quad (13)$$

By employing the same methods, Table 9 presents the ductility values of reinforced concrete columns (test specimens) constructed with confinement reinforcement according to the provisions of AS 3600:2017.

Table 9 Strain ductility of RC column with constant confining pressure (AS3600-2017)

Column Type	I	II	III	IV	V
X3.L4.T4	2.263	2.344	2.292	2.345	2.324
X3.L4.T7	2.291	2.356	2.327	2.340	2.306
X3.L4.T10	2.300	2.343	2.321	2.321	2.307

Column Type	I	II	III	IV	V
X3.L5.T5	2.288	2.341	2.329	2.329	2.321
X3.L5.T7	2.303	2.392	2.326	2.337	2.627
X3.L5.T10	2.324	2.378	2.357	2.394	2.648
X5.L4.T4	1.864	1.908	1.858	1.917	1.869
X5.L4.T7	1.856	1.863	1.838	1.875	1.815
X5.L4.T10	1.911	1.802	1.850	1.796	1.777
X5.L5.T5	1.837	1.846	1.840	1.875	1.842
X5.L5.T7	1.835	1.849	1.852	1.865	1.835
X5.L5.T10	1.820	1.794	1.831	1.789	1.789

Table 9 demonstrates that columns meeting the minimum diameter requirements of AS 3600:2017 exhibit comparable ductility. This suggests that by adhering to the standard confining pressure specified in AS 3600:2017, the desired level of ductility can be achieved, even if the yield stress of the stirrup reinforcement exceeds the specified value.

Table 10 Strain ductility of RC column with constant A_{sh}/b_s (ACI 318-19)

Column Type	I	II	III	IV	V
X3.L4.T4	3.257	4.500	4.727	4.639	5.181
X3.L4.T7	3.238	5.000	5.325	5.095	5.905
X3.L4.T10	3.264	5.695	7.095	7.071	10.000
X3.L5.T5	3.186	4.390	4.491	4.478	6.588
X3.L5.T7	3.222	4.936	5.156	5.156	6.463
X3.L5.T10	3.200	5.724	7.616	7.584	11.242
X5.L4.T4	2.388	3.279	3.497	3.564	3.861
X5.L4.T7	2.392	3.389	3.806	3.774	4.158
X5.L4.T10	2.312	3.457	4.466	4.788	5.698
X5.L5.T5	2.270	3.235	3.420	3.431	3.688
X5.L5.T7	2.363	3.306	3.739	3.782	4.145
X5.L5.T10	2.303	3.427	4.489	4.768	5.722

Table 10 presents the ductility of reinforced concrete columns designed according to ACI 318-2019.

It reveals a range of strain ductility among columns constructed per the ACI 318-2019 standards. This variation in ductility is further depicted in Figure 22.

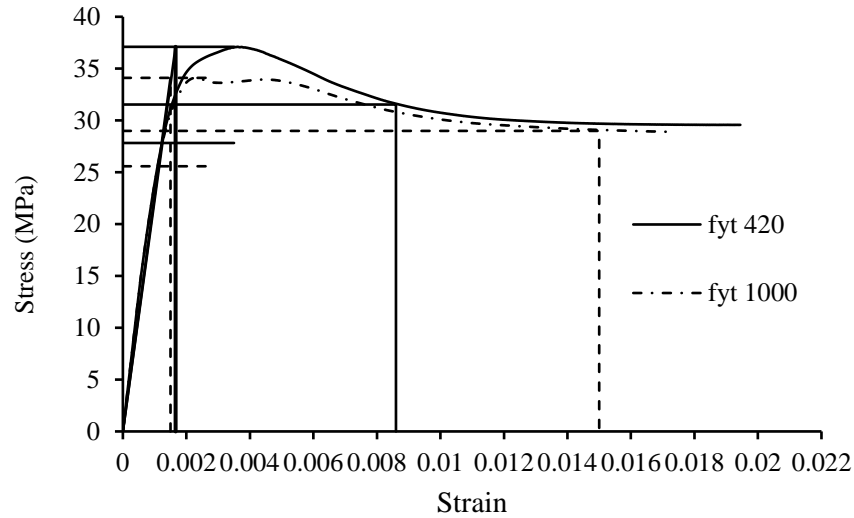


Figure 22 Column Ductility Comparison (ACI 318-2019) between f_{yt} 420 MPa and f_{yt} 1000 MPa
Column Type V f_c 30 MPa

ACI 318-2019 focuses only on the ratio between the column's gross cross-sectional area and its core area for confinement reinforcement. This results in minimal variations in peak stresses among columns designed according to this standard, primarily influenced by lateral stiffness.

The choice of confinement strength (f_{yt}) significantly impacts the ductility of column strain. Higher f_{yt} values, such as 1000 MPa, allow for greater strain of $0.85 f'_c$ compared to lower f_{yt} values like 420 MPa. Consequently, higher f_{yt} values lead to larger strain ductility, as the column can deform more before reaching its ultimate limit.

$$\varepsilon_y \text{ column with } f_{yt} \text{ 420 MPa} > \varepsilon_y \text{ column with } f_{yt} \text{ 1000 MPa}$$

$$\varepsilon_{0.85} \text{ column with } f_{yt} \text{ 420 MPa} < \varepsilon_{0.85} \text{ column with } f_{yt} \text{ 1000 MPa}$$

$$\frac{\varepsilon_{0.85}}{\varepsilon_y} \text{ column with } f_{yt} \text{ 1000 MPa} > \frac{\varepsilon_{0.85}}{\varepsilon_y} \text{ column with } f_{yt} \text{ 420 MPa}$$

$$\mu \text{ column with } f_{yt} \text{ 1000 MPa} > \mu \text{ column with } f_{yt} \text{ 420 MPa}$$

Based on this explanation, it can be concluded that columns designed according to ACI 318-2019 standards, with minimum stirrup variations, exhibit varying levels of strain ductility, despite meeting the same reinforcement requirements.

Figure 23 depicts a contrast in the achievement of strain ductility for columns designed in accordance with the minimum diameter requirements of ACI 318-2019 and AS 3600:2017.

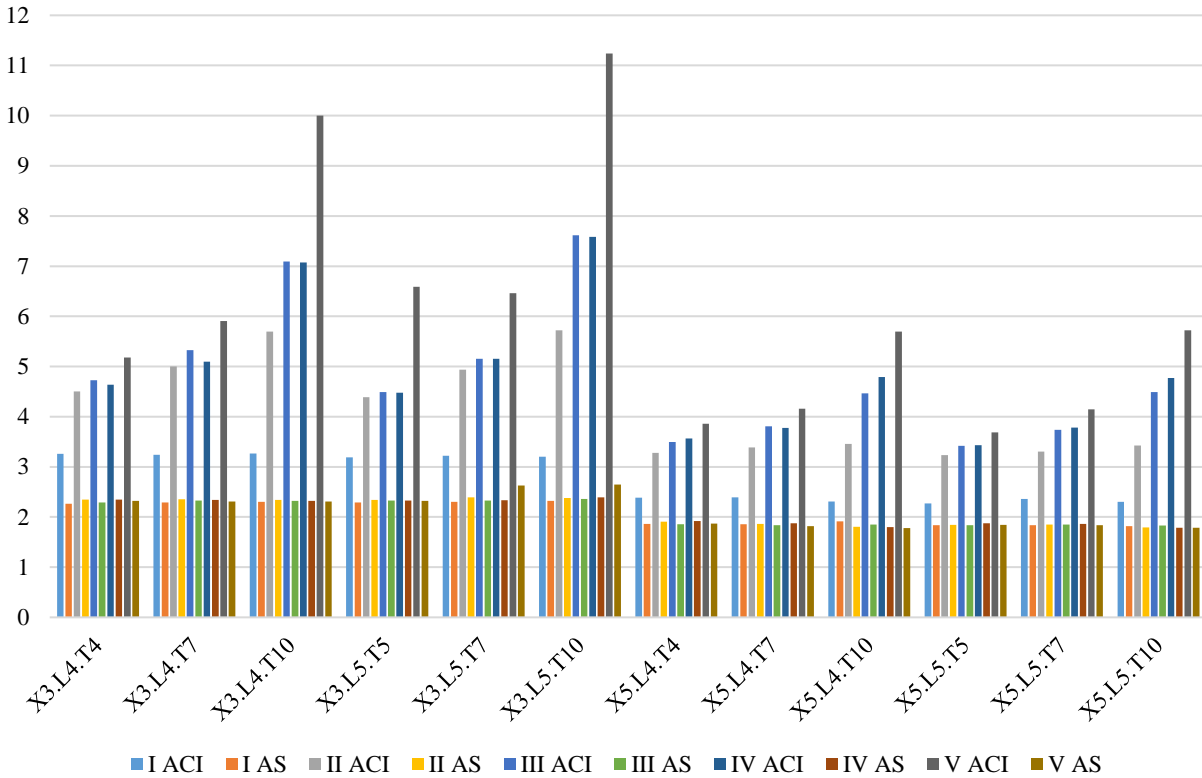


Figure 23 Strain Ductility for Columns Designed in ACI 318-2019 And AS 3600:2017

The examination of Figure 23 provides crucial insights into the structural performance of reinforced concrete columns across diverse design standards. Firstly, columns complying with AS 3600:2017's minimum diameter requirements exhibit consistent ductility, showcasing the reliability of the prescribed confining pressure. Secondly, ACI 318-2019's emphasis on the gross-to-core area ratio influences peak stress uniformity, primarily dictated by lateral stiffness. Additionally, the substantial impact of confinement strength (f_{yt}) on strain ductility is evident, highlighting the role of f_{yt} in enhancing deformation capacity. Lastly, variations in strain ductility among columns designed per ACI 318-2019, despite minimal stirrup differences, suggest nuanced factors at play beyond mere reinforcement quantity.

The ductility of a column in the potential plastic hinge region is typically characterized by an idealized trilinear force-deformation diagram, which comprises three regions: ascending, plateau, and softening. Ductility is commonly evaluated when the peak load decreases to 85% of its capacity. The ductility index (I_{10}) is derived from the energy area beneath the load-strain curve of the column.

The ductility of the RC column is quantified using the I_{10} ductility index, which assesses the energy ratio. This energy is determined by calculating the area under the curve of the axial load (P) versus nominal strain (ϵ). In the case of concentrically loaded RC columns, the nominal strain is equivalent to the axial strain. It is worth noting that the I_{10} ductility index has been employed by Samani et al. (Samani, Attard, and Foster 2015) for evaluating the ductility of RC columns.

The I_{10} considers the yield strain (ϵ_y) and 5.5 times the nominal yield strain ($5.5 \epsilon_y$) for calculation. It measures the ratio of the area under the curve from $5.5 \epsilon_y$ to ϵ_y . An I_{10} index of one represents an elastic-perfectly brittle material, while an I_{10} index of ten corresponds to an elastic-perfectly plastic model. Figure 24 provides a detailed explanation of I_{10} measurement.

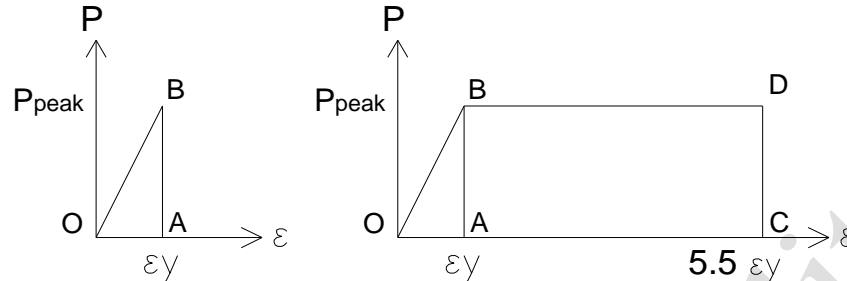


Figure 24 I_{10} ductility index for (a) elastic-perfectly brittle material and (b) elastic-perfectly plastic material.

The ductility index of specimen column I3.L4.T4, designed according to the reinforcement requirements of AS 3600:2017, can be determined using the graphical method depicted in figure 25. The ductility index can then be calculated by evaluating the area under the curve, as expressed in equation (14) below:

$$I_{10} = \frac{\text{Area under curve to } 5.5\epsilon_y}{\text{Area under curve to } \epsilon_y} \quad (14)$$

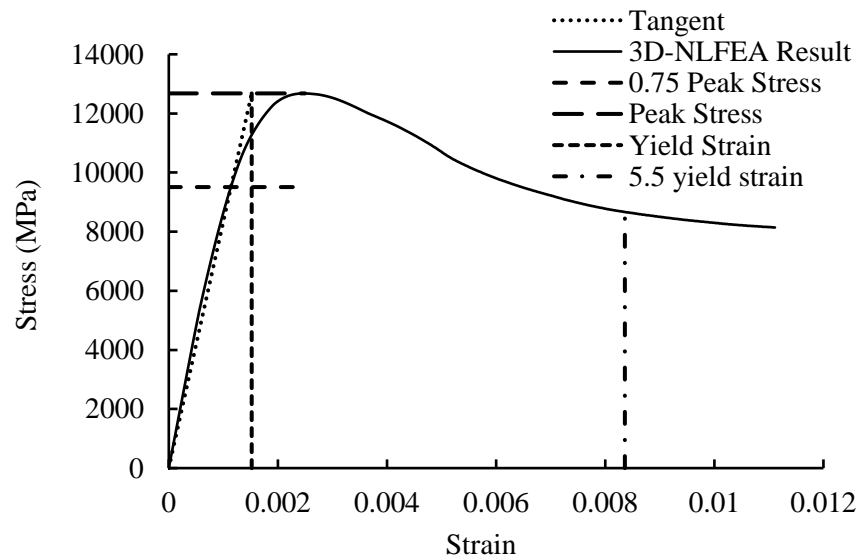


Figure 25 Ductility Index Calculation of Column Type I3.L4.T4 Designed According to AS 3600:2017

Table 11 presents the ductility index of reinforced concrete columns designed in accordance with AS 3600:2017 standards.

Table 11 I_{10} ductility index of RC column with constant confining pressure (AS3600-2017)

Column Type	I	II	III	IV	V
X3.L4.T4	7.1166529	7.4691619	7.3768913	7.47007	7.460995
X3.L4.T7	7.265861	7.4837516	7.456004	7.45562	7.651411
X3.L4.T10	7.2931671	7.5457574	7.4869508	7.511647	7.506907
X3.L5.T5	7.2415735	7.4414874	7.4056108	7.431082	7.344545
X3.L5.T7	7.3034621	7.5651303	7.4445493	7.433756	7.543412
X3.L5.T10	7.3762808	7.5687152	7.5060432	7.589289	7.545897
X5.L4.T4	6.389787	6.811318	6.492846	6.794314	6.747175
X5.L4.T7	6.324716	6.7644	6.461826	6.719558	6.712184
X5.L4.T10	6.761192	6.828948	6.947423	6.787364	6.787051
X5.L5.T5	6.354541	6.68235	6.361365	6.728676	6.607029
X5.L5.T7	6.355158	6.738293	6.437094	6.793737	6.787393
X5.L5.T10	6.360145	6.853521	6.551679	7.018206	6.929423

Table 11 demonstrates that columns (test specimens) designed according to AS 3600:2017 confinement requirements, considering variations in configuration, longitudinal reinforcement yield strength, and transverse reinforcement yield strength, exhibit consistent ductility index (I_{10}). This implies that by adjusting the confinement pressure requirements in accordance with AS 3600:2017 standards, the desired level of ductility can be achieved, even when the confinement yield strength exceeds the code-specified value of 1000 MPa.

Additionally, Table 12 presents the ductility index (I_{10}) of reinforced concrete columns designed according to ACI 318-2019 using the same approach.

Table 12 I_{10} ductility index of RC column with constant A_{sh}/b_s (ACI 318-19)

Column Type	I	II	III	IV	V
X3.L4.T4	8.439448	9.050173	9.0815934	9.0401	8.699055963
X3.L4.T7	8.415725	9.129695	9.2423233	9.059597	9.1530027
X3.L4.T10	8.587081	9.22032	9.3908361	9.363342	9.396854283
X3.L5.T5	8.412246	8.928137	9.0272252	9.013962	8.006013257
X3.L5.T7	8.415967	9.103203	9.1636645	9.195624	9.818547776
X3.L5.T10	8.523426	9.217122	9.4667608	9.580538	9.422981565
X5.L4.T4	7.520316	8.659733	8.689585	8.70404	8.81442026
X5.L4.T7	7.611878	8.778546	8.940826	8.86798	8.637399957
X5.L4.T10	7.507538	8.713933	9.081247	9.201794	9.323091093
X5.L5.T5	7.534136	8.583219	8.670677	8.655809	8.763608863
X5.L5.T7	7.551625	8.698117	8.891821	8.859737	8.966636908
X5.L5.T10	7.591402	8.689093	9.280597	9.151548	9.127884141

Table 12 demonstrates consistent ductility index for columns designed per ACI 318-2019, regardless of variations in configuration and yield strength of reinforcement. This suggests that achieving the desired ductility index in high-strength columns can be accomplished by maintaining uniform confinement strength across different yield stresses.

Figure 24 illustrates a comparison of the ductility index achievement for columns designed to adhere to the minimum diameter specifications of ACI 318-2019 and AS 3600:2017.

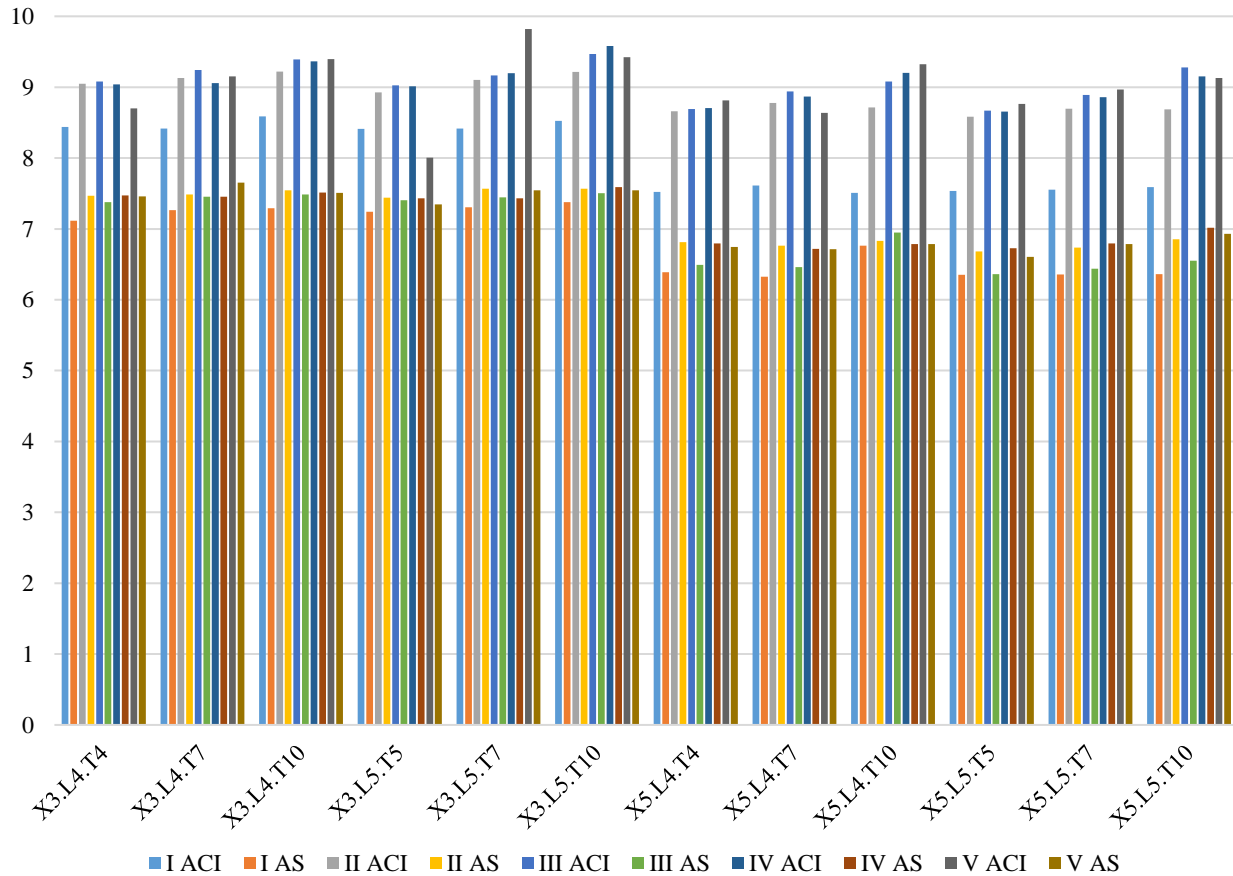


Figure 26 Ductility Index Calculation of Column Type I3.L4.T4 Designed According to AS 3600:2017

The bar graph in Figure 26 provides compelling insights into the comparative performance of columns designed under AS 3600:2017 and ACI 318-2019 standards. Columns conforming to AS 3600:2017 exhibit consistent ductility index across varied configurations and reinforcement yield strengths, emphasizing the reliability of achieving desired ductility through adjusted confinement pressure. Meanwhile, ACI 318-2019-designed columns consistently maintain a uniform ductility index, underscoring the importance of a consistent confinement strength for desired performance in high-strength columns.

Multiple studies (Foster and Attard 2001; Foster, Stephen, and Attard 1997) have proposed a relationship between column ductility and the confinement parameter $k_e \rho_s f_{yt} / f'_c$ %. In their work, Attard and Foster (Foster, Stephen, and Attard 1997) established a regression equation (15) to predict the ductility index based on this parameter:

$$I_{10} = 1,9 \ln (1000 k_e \rho_s f_{yt} / f'_c) \quad (15)$$

Figure 27 (a) shows the correlation between confinement parameters and I_{10} values of examined columns, while Figure 24 (b) displays the percentage of errors in the Attard and Stunge model.

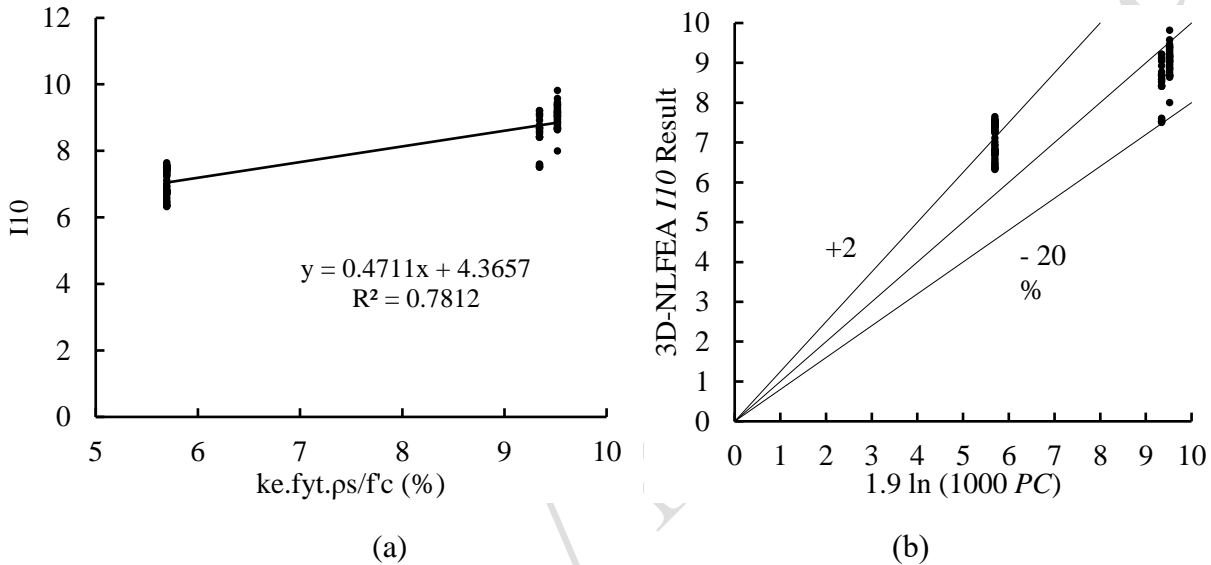


Figure 27 (a) Correlation between Confinement Parameters and I_{10} Values from 3D-NLFEA and (b) Comparison of I_{10} Results: 3D-NLFEA vs. Constitutive Model

Figure 27 (b) highlights the limitations of the confinement parameters which are based solely on $k_e \rho_s f_{yt}$ dan f'_c factors. In this test, the specimens are subjected to the same confinement pressure, resulting in similar confinement parameters for specimens with the same value. However, the test results reveal a range of ductility indices due to the influence of longitudinal and confinement reinforcement yield stresses. To approach the ductility index results of the column specimens, new confinement parameters have been proposed. These parameters are represented by the equation 16.

$$\text{Proposed Confinement Parameter (PC)} = k_e \rho_s \frac{f_y f_{yt}}{(f'_c)^2} \quad (16)$$

Figure 28 illustrates the relationship between the proposed confinement parameter and the achieved ductility index of the test specimens.

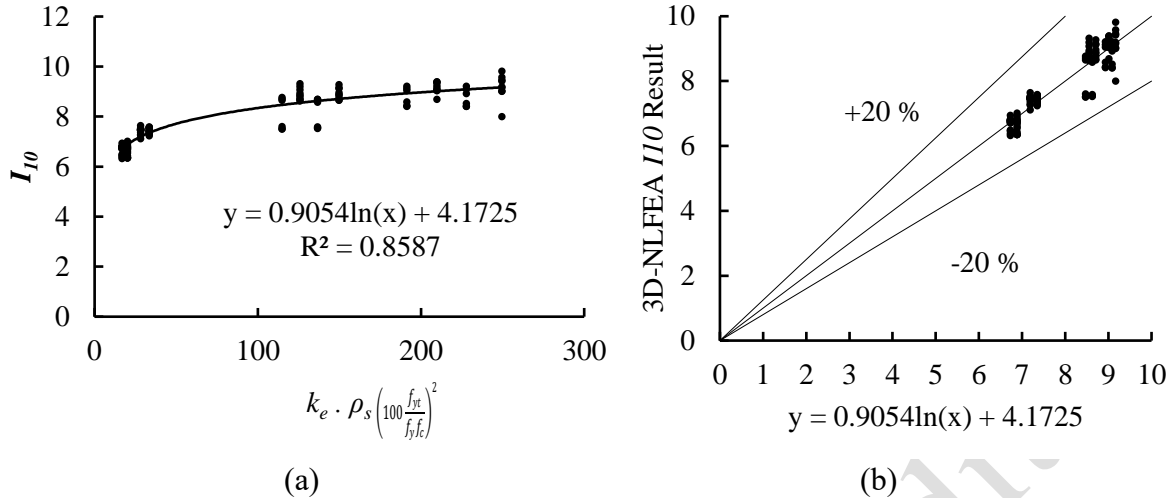


Figure 28 Relationship between Confinement Parameters with 3D-NLFEA I_{10} Result
 (b) Comparison of Test Specimen Ductility Index with Proposed Confinement Parameters

Equation 17 presents the proposed confinement parameters for predicting the I_{10} .

$$\text{Proposed } I_{10} = 0.9 \ln \left(k_e \rho_s \frac{f_y f_{yt}}{(f_c)^2} \right) + 4.17 \quad (17)$$

4. Conclusions

This study extensively investigated axially loaded square-reinforced concrete columns comprising normal-strength concrete and high-strength confinement rebars with diverse configurations. The study findings are summarized as follows:

1. Columns designed according to AS 3600:2017 standards consistently demonstrated a mean strain ductility range of 1.78 to 1.92, indicating relatively minor variation under identical minimum confining pressure.
2. In contrast, columns designed per ACI 318-2019 standards exhibited a wider range of strain ductility, ranging from 2.27 to 11.24, despite comparable Ash values.
3. This finding indicates that the utilization of high-strength steel confining rebars (exceeding 800 MPa) in columns adhering to minimum confinement requirements resulted in a mean ductility index of 7.93, ensuring the columns' safe and reliable performance.
4. Additionally, the proposed predictive model for the column's ductility index demonstrated an average deviation of 3.53%, underscoring its accuracy and reliability in ductility estimation.

These quantified results offer insights into the variations in strain ductility, shedding light on the nuanced impacts of different design standards and reinforcement configurations on the ductility and performance of reinforced concrete columns.

However, several key considerations emerged during study, which must be addressed:

1. An increase in the yield stress of steel bars may lead to a reduction in ductility, which warrants attention in future research and design considerations. Additionally, the primary purpose of

using transverse bars in reinforced concrete (RC) columns is to enhance ductility rather than strength, aligning with the fundamental objectives of reinforced concrete design.

2. While the study provides valuable insights, it's important to exercise caution in asserting that its results can directly influence or alter existing building code regulations. Emphasis is placed on the research aiming to inform rather than dictate regulatory changes. The practical implications of utilizing high-strength steel bars, including potential increases in construction costs and implications for the strong column-weak beam condition, suggest the need for further research and careful evaluation in real-world applications.
3. Finally, the basic assumption underlying valid building codes regarding plastic hinge formation in moment frames during strong earthquakes highlights the importance of considering seismic design principles in structural engineering practice. If in moment frames, the ductility demand of the column exceeds that of the beam, the formation of the plastic moment is prioritized in columns. This can lead to the unwanted phenomenon of weak column-strong beam during earthquakes.
4. Additionally, the use of high-strength rebars has two major drawbacks: an increase in construction costs and potential shortages when supplying the construction materials. These issues can result in difficulties in executing the project. Despite the valuable insights provided by this research, it's important to recognize that its results alone cannot alter established regulations of accredited building codes. This paper serves as a technical note rather than a means to change regulations.

In conclusion, this research enriches understanding regarding the impact of high-strength reinforcement on the ductility of normal-strength reinforced concrete columns, providing valuable insights that can guide future research efforts and inform engineering decision-making processes.

Acknowledgments

My gratitude to Mr. Saifuddin and Mrs. Heni for providing the funds to complete this research.

References

- ACI 318. (2019). *Building Code Requirements for Structural Concrete (ACI 318-19) Commentary on Building Code Requirements for Structural Concrete (ACI 318R-19) Reported by ACI Committee 318*. https://www.concrete.org/Portals/0/Files/PDF/Previews/318-19_preview.pdf.
- Alavi-Dehkordi, Sayedmahdi, and Davood Mostofinejad. (2018). "Behavior of Concrete Columns Reinforced with High-Strength Steel Rebars under Eccentric Loading." *Materials and Structures* 51(6): 145.
- AS:3600. (2017). "Concrete Structures (Draft for Public Comment Australian Standard)." 1(June). <https://www.mbawa.com/wp-content/uploads/2017/07/DR-AS-3700-2017-Masonry-structures.pdf>.
- Cai, Zhong-Kui, Zhenyu Wang, and T.Y Yang. (2018). "Experimental Testing and Modeling of Precast Segmental Bridge Columns with Hybrid Normal-and High-Strength Steel Rebars."

Construction and Building Materials 166: 945–55.

- Ding, Hongyan, Yuan Liu, Chao Han, and Yaohua Guo. (2017). “Seismic Performance of High-Strength Short Concrete Column with High-Strength Stirrups Constraints.” *Transactions of Tianjin University* 23: 360–69.
- Foster, Stephen J, and Mario M Attard. (2001). “Ductility of High Strength Concrete Columns.” 127(January): 28–34.
- Foster, James Stephen, and Mario M. Attard. (1997). “Experimental Test on Eccentrically Load High Strength Concrete Columns.” *Structural Journal* 94(3): 295–303.
- Hung, Chung Chan, and Chen Yu Chueh. (2016). “Cyclic Behavior of UHPFRC Flexural Members Reinforced with High-Strength Steel Rebar.” *Engineering Structures* 122: 108–20. <http://dx.doi.org/10.1016/j.engstruct.2016.05.008>.
- Kamaruddin, Kurniawan Setiadi, Iswandi Imran, and Maulana Derry Imansyah. (2018). “Application of High Strength Reinforcing Bars in Earthquake-Resistant Structure Elements.” 02015: 1–10.
- Kim, Min-Jun et al. (2021). “Effect of Configuration and Yield Strength of Transverse Reinforcement on Lateral Confinement of RC Columns.” *Applied Sciences* 11(15): 6696.
- Moehle, Jack P, John D Hooper, Dominic J Kelly, and Thomas R Meyer. NEHRP Seismic Design Technical Brief *Seismic Design of Cast-in-Place Concrete Diaphragms, Chords, and Collectors: A Guide for Practicing Engineers (NIST GCR 10-917-4)*. www.curee.org.
- Ou, Yu Chen, and Dimas P. Kurniawan. (2015). “Shear Behavior of Reinforced Concrete Columns with High-Strength Steel and Concrete.” *ACI Structural Journal* 112(1): 35–46.
- Piscesa, Bambang, Mario M. Attard, Dwi Prasetya, and Ali K. Samani. (2019). “Modeling Cover Spalling Behavior in High Strength Reinforced Concrete Columns Using a Plasticity-Fracture Model.” *Engineering Structures* 196(June): 109336. <https://doi.org/10.1016/j.engstruct.2019.109336>.
- Piscesa, Bambang, Mario M Attard, and Ali Khajeh Samani. (2018). “3D Finite Element Modeling of Circular Reinforced Concrete Columns Confined with FRP Using a Plasticity Based Formulation.” *Composite Structures* 194: 478–93.
- Samani, Ali Khajeh, Mario M. Attard, and Stephen J. Foster. (2015). “Ductility in Concentrically Loaded Reinforced Concrete Columns.” *Australian Journal of Structural Engineering* 16(3): 237–50.
- Seliem, Hatem M. et al. (2009). “Bond Characteristics of ASTM A1035 Steel Reinforcing Bars.” *ACI Structural Journal* 106(4): 530–39.
- Sreevalli, I Yamini. (2021). “A Review on Progressive Collapse of Reinforced Concrete Flat Slab Structures.” *Civil Engineering Infrastructures Journal* 54(1): 181–94.
- Ulfa, Anis Aulia et al. (2020). “Parametric Studies on the Ductility of Axial Loaded Square Reinforced Concrete Column Made of Normal-Strength Concrete (NSC) and High-Strength Steel Confining Rebar (HSSCR) with Various Ties Configuration.” *E3S Web of Conferences*

156: 0–6.

Wang, Peng, Qingxuan Shi, Feng Wang, and Qiuwei Wang. (2020). “Seismic Behaviour of Concrete Columns with High-Strength Stirrups.” *Earthquake and Structures* 18(1): 15–25.

Accepted / Not Edited